Development 109, 533–551 (1990)
Printed in Great Britain © The Company of Biologists Limited 1990



# Structural and compositional divergencies in the extracellular matrix encountered by neural crest cells in the white mutant axolotl embryo

R. PERRIS[1,*], J. LÖFBERG[1], C. FÄLLSTRÖM[1], Y. VON BOXBERG[2], L. OLSSON[1] and D. F. NEWGREEN[3]

[1]*Department of Zoology, Uppsala University, Box 561, S-751 22 Uppsala, Sweden*
[2]*Max-Planck Institut für Entwicklungsbiologie, Spemannstrasse 35, D-7400 Tübingen, FRG*
[3]*Department of Pediatrics, Westmead Hospital, Westmead, 2145, N. S. W. Australia*

* Present address for correspondence: Developmental Biology Center, University of California Irvine, Irvine, CA 92717, USA

## Summary

**The skin of the white mutant axolotl larva is pigmented differently from that of the normal dark due to a local inability of the extracellular matrix (ECM) to support subepidermal migration of neural crest-derived pigment cell precursors. In the present study, we have compared the ECM of neural crest migratory pathways of normal dark and white mutant embryos ultrastructurally, immunohistochemically and biochemically to disclose differences in their structure/composition that could be responsible for the restriction of subepidermal neural crest cell migration in the white mutant axolotl. When examined by electron microscopy, in conjunction with computerized image analysis, the structural assembly of interstitial and basement membrane ECMs of the two embryos was found to be largely comparable. At stages of initial neural crest cell migration, however, fixation of the subepidermal ECM *in situ* with either Karnovsky–ruthenium red or with periodate–lysine–paraformaldehyde followed by ruthenium red-containing fixatives, revealed that fibrils of the dark matrix were significantly more abundant in associated electron-dense granules. This ultrastructural discrepancy of the white axolotl ECM was specific for the subepidermal region and suggested an abnormal proteoglycan distribution. Dark and white matrices of the medioventral migratory route of neural crest cells had a comparable appearance but differed from the corresponding subepidermal ECMs. Immunohistochemistry revealed only minor differences in the distribution of fibronectin, laminin, collagen types I, and IV, whereas collagen type III appeared differentially distributed in the two embryos. Chondroitin- and chondroitin-6-sulfate-rich proteoglycans were more prevalent in the white mutant embryo than in the dark, especially in the subepidermal space. Membrane microcarriers were utilized to explant site-specifically native ECM for biochemical analysis. Two-dimensional gel electrophoresis of these regional matrices revealed a number of differences in their protein content, principally in constituents of apparent molecular masses of 30–90 000. Taken together our observations suggest that local divergences in the concentration/assembly of low and high molecular mass proteins and proteoglycans of the ECM encountered by the moving neural crest cells account for their disparate migratory behavior in the white mutant axolotl.**

Key words: axolotl embryo, extracellular matrix, ultrastructure, immunohistochemistry, gel electrophoresis, neural crest.

## Introduction

During embryonic development, the pigment pattern of the vertebrate skin is established by migration of prospective pigment cells from their original position within the neural crest to distant subepidermal sites (Le Douarin, 1984; Newgreen and Erickson, 1986; Löfberg *et al.* 1989*a*). In order to reach these eventual locations, pigment cell precursors migrate dorsolaterally entering a cell-free space between the epidermis and somites. This subepidermal migratory pathway is filled with an intricate extracellular matrix (ECM) which is thought to support migration and participate in the guidance of neural crest cells as they move through the tissue environment (Löfberg *et al.* 1980; Spieth and Keller, 1984; Newgreen and Erickson, 1986; Martins-Green and Erickson, 1987; Dufour *et al.* 1987; Perris and Bronner-Fraser, 1989*a*; Löfberg *et al.* 1989*a*). Moreover, a previous study from our group has shown that a developmental alteration of the ECM surrounding the neural crest is a timing factor for the initiation of neural crest cell migration (Löfberg *et al.* 1985).

The white mutant axolotl is a naturally occurring variant of the species, which results from the homo-

zygous recessive allele combination d/d. The phenotype of the normal dark embryo is determined by the dominant allele D, and hence homozygous (DD) as well as heterozygous (Dd) animals show the dark, wild-type skin pigmentation (Frost and Malacinski, 1980). In contrast, the white mutant axolotl exhibits a restricted skin pigmentation (Figs 1 and 2), arising from the inability of the embryonic epidermis to support dorsolateral migration of neural crest-derived pigment cell progenitors (Dalton, 1950; Bogomolova and Korochkin, 1973; Keller *et al.* 1982). Medioventral migration of neuronal and neural support-cell precursors, however, does occur as revealed by the apparently normal formation of dorsal root ganglia (Borack, 1972), and development of the larvae to long-lived and fertile adults.

Recently, we discovered that the defect of the white axolotl epidermis, which is particularly noticeable in the trunk region, resides in the ECM produced by this tissue (Epperlein *et al.* 1986; Löfberg *et al.* 1989*b*). Surprisingly, however, while the ECM of the subepidermal space of the white embryo is nonpermissive for neural crest cell movement at developmental stages corresponding to the onset of migration, it acquires motility-promoting capacities at stages corresponding to advanced neural crest cell movement (Löfberg *et al.* 1989*b*). Thus, the genetically governed anomaly appears to functionally rest upon an asynchronous development of the neural crest cells *versus* the subepidermal ECM, such that this matrix attains migration-stimulating capacities when neural crest cells have lost their ability to respond to this environmental signal.

In the present investigation, we have undertaken an ultrastructural, immunohistochemical and biochemical characterization of the ECMs of normal dark and white mutant axolotl embryos prior to and during neural crest cell migration. The results suggest that the regional ECM of these two axolotl variants differs in structure as well as molecular composition, and that this divergent matrix organization may be responsible for the restricted subepidermal migration in the white axolotl mutant.

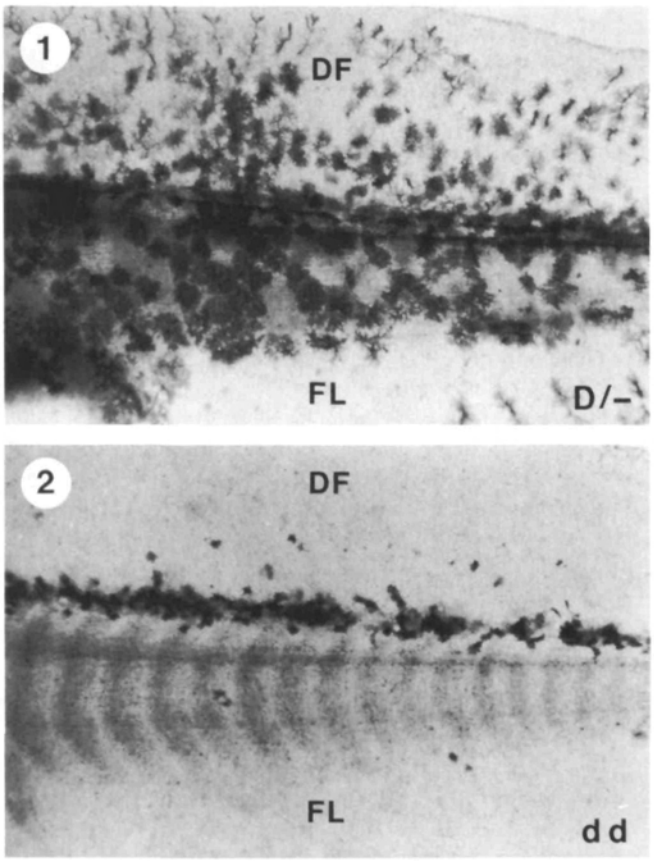


**Fig. 1.** Macrograph of the trunk region of a dark axolotl (D/−) at stage 40–42 showing the pronounced spreading of pigment cells on the flank (FL) and dorsal fin (DF) of the larva. ×75.

**Fig. 2.** Comparable macrograph to that shown in Fig. 1 illustrating the restricted pigment cell migration in the white axolotl mutant (dd). Conspicuously, the majority of the pigment cells remain compacted on the dorsal surface of the neural tube. ×75.

## Materials and methods

### *Light microscopy*

Normal dark and white mutant axolotl embryos (*Ambystoma mexicanum*) at developmental stages 29–31 (Bordzilovskaya and Dettlaff, 1979) were fixed in modified Karnovsky fixative, 1.5% glutaraldehyde and 1.5% paraformaldehyde in 0.1 M phosphate buffer pH 7.2, for 5 h at room temperature or overnight at 4°C. Fixed embryos were rinsed in 0.2 M cacodylate buffer, cut transversely level with the 3rd trunk segment to allow satisfactory penetration of the postfixative, and incubated in cacodylate buffered 1% $OsO_4$ containing 400 ppm ruthenium red, for 4–6 h at 4°C. Stained specimens were extensively rinsed, dehydrated in a graded series of ethanol and embedded in Epon according to conventional procedures. Semi-thin sections, about 2–3 μm, were cut on a LKB ultramicrotome and mounted on methanol-washed slides. In order to enhance the contrast of ruthenium red-precipitated ECM structures, the sections were stained with silver and gold salts according to the method of Löfberg and Ahlfors (1978).

### *Electron microscopy and morphometry by computer-aided image analysis*

Dark and white mutant embryos were fixed in modified Karnovsky fixative at selected developmental stages (30–35), with or without ruthenium red, or in periodate–lysine–paraformaldehyde (PLP; McLean and Nakane, 1974) followed by postfixation with ruthenium red (see below), and prepared for scanning (SEM) and transmission (TEM) electron microscopy as whole or freeze-fractured specimens according to previously described procedures (Löfberg *et al.* 1980; 1985).

For fixation of the subepidermal ECM *in situ*, a piece of the lateral flank epidermis (between 4th and 9th somite) was excised from the embryo following a previously devised microsurgical procedure (Löfberg *et al.* 1985; Perris and Löfberg, 1986). Ruthenium red-containing Karnovsky fixative was then flushed with a Pasteur pipette into the exposed subepidermal region in order to obtain instantaneous fixation of the local ECM. Alternatively, to improve the preservation

of carbohydrate moieties of matrix components, the subepidermal compartment of living embryos was flushed with PLP prior to the ruthenium red-precipitation. PLP-flushed embryos were kept in the same ice-cold fixative for 2–6 h, rinsed in 0.1 M cacodylate buffer and further fixed overnight or longer in 1.0 % glutaraldehyde in the same buffer at 4 °C. The embryos were then rinsed in buffer and postfixed in cacodylate-buffered 1 % $OsO_4$ containing 0.05 % ruthenium red for 1 h at 4 °C, and finally prepared for SEM according to routine procedures. In some specimens, individual somite blocks were dissected out and mounted separately to allow SEM examination of the perineural ECM. Subepidermal and perineural ECMs of 7 embryos of each genotype (D/− and dd) and stage (30 and 35) were subjected to morphometry by computerized image analysis. In each embryo, 10 areas each of subepidermal and perineural interstitial ECM were chosen at random and photographed (magnification ×7800) in the SEM. The micrographs were then analyzed with a Crystal image processor (Quantel, Ltd). In each series of 10 micrographs, the projected area and length of the fibrils were measured for 20–26 individual fibril segments. The ratio between projected fibril area and fibril length was adopted as a parameter indicating the degree of granulation of the fibrils. Since normal distribution could not be assumed, the results are presented as median values with 95 % confidence limits. The non-parametric Mann-Whitney U-test was used in pairwise comparisons to establish whether median values significantly differed between groups.

Embryos to be treated with enzyme for characterization of ECM components in ultrathin sections were fixed in modified Karnovsky fixative at 4 °C overnight. They were then rinsed in 0.2 M phosphate buffer for 1–2 h at room temperature and cut transversely to allow penetration of the enzyme. Once rinsed, the embryos were incubated in 0.1 M phosphate buffer, pH 5.2, containing 100 TRU $ml^{-1}$ *Streptomyces* hyaluronidase (Miles; Derby and Pintar, 1978) for 2 h at 37 °C. Control embryos were incubated in the same buffer but lacking enzyme. During the subsequent rinsing steps, treated and control embryos were transferred from the phosphate buffer to 0.1 M cacodylate buffer pH 7.4 and postfixed 1 % $OsO_4$/ruthenium red. Counterstaining was performed using uranyl acetate and lead citrate. Ultrathin sections from specimens treated with enzyme, and control specimens were cut 200–300 μm caudal to the cut edge of the embryos in order to obtain sections from comparably stained and digested trunk areas. Sections were cut at an approximate thickness of 50–70 nm.

### *Antibodies*

The various antibodies used in this study were obtained as follows: affinity-purified antisera against axolotl, *Xenopus* and human fibronectins from Drs Jean-Claude Boucaut, Laboratoire de Biologie Experimentale, Universite Rene Descartes, Paris, France, Richard Hynes, Department of Biology, MIT, Cambridge, MA, and Antti Vaheri, Department of Pathology, University of Helsinki, Finland; affinity-purified antisera against collagen types I and III isolated from bovine and chick from Drs Daniel Hartmann, Centre de Radioanalyse, Institute Pasteur de Lyon, Lyon, France and Charles Little, Department of Anatomy and Cell Biology, University of Virginia, Charlottesville, VA; affinity-purified antisera recognizing the globular domains of human collagen type IV from Dr Jörgen Wieslander, Biocarb AB, Lund, Sweden. Cross-reactivity of the anti-collagen antisera for the corresponding antigens in the axolotl was ascertained by Western blot analysis which showed that: the anti-collagen type I antiserum recognized two major bands at 95 000, and 145 000 $M_r$, and a doublet at 195 000–220 000 $M_r$; the anti-collagen type III antiserum recognized a single band at 105 000 $M_r$; the anti-collagen type IV antiserum to the NC1 domain labelled a major band at 175 000 $M_r$. An antiserum against laminin (purified from EHS mouse tumor) was received from Dr Brigid Hogan, Medical Research Council, Mill Hill Laboratories, London UK. Mouse monoclonal antibodies reactive with the chondroitin-6-sulfate, chondroitin-4-sulfate, unsulfated chondroitin and keratan sulfate moieties of proteoglycans were donated by Dr Bruce Caterson, Department of Biochemistry, West Virginia University, Morgantown, WV.

### *Immunohistochemical procedures*

Normal dark and white mutant embryos at developmental stages 30 and 35 were precooled for 1 h at 4 °C and subsequently immersed in ice-cold Saint-Marie fixative (Saint-Marie, 1962), for 18 h at 4 °C. Fixed embryos were rinsed in 0.1 M phosphate buffer pH 7.4 and cut transversely at the level of the 3rd trunk segment in order to facilitate penetration of the embedding medium. Embryos were then dehydrated through a graded series of cooled ethanol washes, passed through precooled xylene, brought to room temperature and embedded in paraffin wax. Serial transverse and longitudinal sections were cut on LKB-Historange microtomes at an approximate thickness of 6 μm. Transverse sections were cut simultaneously from dark and white mutant embryos on two different microtomes, ordinarily between the 4th and 8th segment. 'Dark and white' sections were mounted adjacent to each other on albuminized slides.

Sections to be immunolabelled were deparaffinized, washed thoroughly in 0.1 M phosphate buffer pH 7.4, and either incubated directly with antibodies or treated with different enzymes prior to immunostaining. For staining with antisera directed against collagen types I–IV, sections were incubated with 200 i.u. $ml^{-1}$ of bovine testicular hyaluronidase (Sigma) in Earle's balanced salt solution for 1 h at 37 °C. After subsequent washing, primary antibodies were applied at dilutions 1:20–1:40. Incubation with anti-laminin antibodies was preceded by digestion with collagenase type III (Sigma) in Earle's balanced salt solution, 250 i.u. $ml^{-1}$ for 1 h at 37 °C. The anti-laminin antiserum was applied at 1:40–1:80 dilutions. The proteoglycan epitopes identified by antibodies directed against the characteristic chondroitin isomers were generated by treating sections with 0.2 i.u. $ml^{-1}$ chondroitinase ABC (Sigma) in 0.1 M bicine buffer (Calbiochem) pH 8.0 for 1 h at 37 °C (Caterson *et al.* 1987). Antibodies against the proteoglycan determinants were used at final dilutions of 1:50. The anti-fibronectin antiserum was applied at concentrations of 1:80–1:160. All incubations with primary antibodies were performed at 4 °C overnight. Biotinylated or fluorescein/rhodamine-conjugated secondary antibodies specific for the various immunoglobulin types (DAKO-PATTS, Denmark; EY-Laboratories Inc.; Bio-Yeda; Amersham) were subsequently applied at dilutions 1:80–1:100 for 1 h at 37 °C. When biotinylated secondary antibodies were employed, visualization of the antibody–antigen binding was accomplished by further incubation of the sections with a streptavidin–fluorescein complex (Amersham), 1:160 for 1 h at room temperature. Stained sections were finally mounted in either a glycerol/glycine-Cl-buffered mixture containing 2 mg $ml^{-1}$ 1,4,-diazabicyclo(2,2,2)octane (DABCO; Sigma), pH 8.0, or in a mounting medium prepared by mixing 2.4 g Mowiol 4-88 (Calbiochem), 6.0 g glycerol, 2 ml 0.2 M Tris–HCl buffer and 6 ml $H_2O$ to give the final pH 8.5. Controls were performed by preincubation with antigens

(when available), omission of primary antibodies in the first incubation step, or replacement of primary antibodies with appropriate nonimmune globulins.

### *Polyacrylamide gel electrophoresis*

Pieces of sterile polycarbonate filter membranes (Nuclepore; pore size 0.04 μm), measuring about 0.2×0.4 mm were cut from whole filter sheets and used as microcarriers. These were inserted microsurgically into the neural crest migratory pathways of living embryos according to a previously described procedure (Löfberg *et al.* 1985; Perris and Löfberg, 1986). After a conditioning period in the embryo, the membrane microcarriers bearing regional ECM that had become adsorbed onto their surfaces *in situ* were explanted and transferred to a labelling buffer (140 mM NaCl, 5 mM KCl, 6 mM $NaHCO_3$, 1.5 mM $CaCl_2 \times 2\ H_2O$; pH 7.5).

For one-dimensional gel electrophoresis, ECM-covered microcarriers were centrifuged and resuspended in 10 μl of the same labelling buffer. A volume of 10 μl of $^{35}$S-labelling reagent ($^{35}$SLR, Amersham), dissolved in benzene and corresponding to an activity of 10 μCi, was then added to the matrix samples. The samples were incubated for 30 min with $^{35}$SLR, and thereafter another 20 μl volume of labelling buffer was added, followed after 5 min by 200 μl Eagle's balanced salt solution. The labelled microcarriers were then centrifuged and the ECM materials attached to their surfaces solubilized in a small volume of SDS-containing buffer (0.8 g Tris, pH 6.8; 10.0 g glycerol; 5.0 g SDS; 5.0 g mercaptoethanol in 100 ml $H_2O$). Solubilized material, corresponding to matrix material adsorbed *in vivo* and explanted on 15–20 microcarriers, was run on 0.1 mm thick 7.5 % polyacrylamide gels at a constant current of 2.0 mA for 1.5 h. After separation, the gels were fixed for 10 min in 45 % ethanol/10 % acetic acid, washed in 50 % ethanol and dried. Finally, gels were exposed to X-ray films (Hyperfilm B-max; Amersham) at −70 °C for a period of 1–3 weeks.

For two-dimensional polyacrylamide gel electrophoresis, ECM-covered microcarriers were solubilized in lysis buffer (8.5 M urea, 5 % mercaptoethanol, 2 % Servalyte 5–8), with or without addition of 2 % Triton X-100. Non-equilibrium electrofocusing was performed in microtube gels prepared using microcapillaries (0.55×60 mm). Gels were loaded with 3.0 μl of matrix homogenates and run at a constant current setting of 20 μA/gel for about 30 min, followed by 2.5 h at 220 V, and finally 30 min at 400 V. Matrix samples were then coupled to $^{35}$SLR by the following procedure: focusing gels were fixed in 40 % methanol/10 % acetic acid for 10 min, washed twice in distilled $H_2O$ (2 min), then twice in labelling buffer. In parallel, a sample of 10 μl of $^{35}$SRL solution in benzene (about 10 μCi) per tube gel was pipetted into an Eppendorf reaction vial. The benzene solvent was dried off with a gentle stream of dry nitrogen, the reagent was redissolved in 10 μl of DMSO, and the $^{35}$SRL solution was instantly added to the tube gel. The gel had meanwhile been immersed in a droplet (20 μl) of labelling buffer. The reaction was then allowed to progress for 1 h at room temperature. Eventually, a volume of 100 μl of labelling buffer was added, and after 5 min the gels were fixed and stained with Coomassie Brilliant Blue, R 250 as previously described (Neukirchen *et al.* 1982; von Boxberg, 1988). Tube gels were then run for the second dimension SDS gel electrophoresis as described above (Neukirchen *et al.* 1982; von Boxberg, 1988). Completed electrophoresis gels were fixed and analyzed autoradiographically as described for the one-dimensional electrophoresis.

## Results

### *General ultrastructural features of basement membranes and subepidermal ECMs of dark and white embryos*

At stages of initial neural crest cell migration, the cell-free region surrounding the premigratory neural crest cord in dark and white embryos was filled with a dense granulo-fibrillar ECM network (Figs 5 and 6). In contrast, the intercellular spaces within the premigratory neural crest cord were conspicuously poor in extracellular material (Figs 7 and 8). Migrating neural crest cells

**Fig. 3.** Stage of advanced neural crest (NC) cell migration in the axial region of a dark embryo as observed by SEM. In several of the clefts between somites (S), neural crest cells migrating ventrally can be seen aligned along the fissures of the clefts (*thick arrows*). Other neural crest cells, starting their emigration level with the midportion of the somites, appear to proceed ventrally on lateral somite surface (*thin arrow*). Two pigment cell aggregates (Epperlein and Löfberg, 1984) can be seen on the dorsal neural tube (*asterisks*). The anterior portion of the embryo is to the left in the micrograph. ×180.

**Fig. 4.** SEM micrograph showing the midtrunk neural crest cord of a white mutant embryo at stages of advanced neural crest cell migration. Although numerous basal neural crest cells have moved medioventrally, no cells can be seen on the lateral somite surfaces or within the intersomitic clefts (compare with dark embryo Fig. 3). The characteristic pigment cell-containing aggregates (*asterisks*) that form along the neural crest cord are conspicuous. Same orientation of the embryo as in Fig. 3. ×200.

**Fig. 5.** Light microscopic cross-section of a normal dark embryo at stage of advanced neural crest cell migration (stage 34–35). The section shows a ruthenium red-treated embryo where staining of the ECM was further enhanced by sequential silver and gold labelling (see Materials and methods). Neural crest cells migrating dorsolaterally (*upper arrow*) enter the subepidermal fibrillar matrix network (F) suspended between the epidermis (EP) and the lateral somites (S). Medioventrally migrating cells (*lower arrow*) move along the lateral neural tube (NT) surface. ×500.

**Fig. 6.** Transverse section through the midtrunk region of white mutant embryo at advanced phases of neural crest cell migration (stage 34–35). The first neural crest cells to emigrate, ordinarily the ones located ventrally in the cord, proceed exclusively medially entering the path between neural tube and somites (S). A large number of neural crest cells remain compacted on the dorsal aspect of the neural tube. EP=epidermis; ×500.

**Fig. 7.** SEM micrograph showing the dorsal subepidermal compartment of a cryofractured dark embryo. While still within the cord, premigratory neural crest cells establish connections with the subepidermal ECM network by means of their filopodial processes (arrows indicating presumed sites of contact). The spaces between the neural crest cells of the original cord appear strikingly devoid of interstitial ECM fibrils (*asterisk*; compare with Fig. 8). ×3000.

**Fig. 8.** TEM micrograph showing a subepidermal area similar to that indicated in Fig. 7. Ruthenium red-precipitated ECM material is abundant in the cell-free subepidermal space between the premigratory neural crest cells and the epidermis (Ep), whereas spaces between two adjacent neural crest cells in the premigratory cord are virtually empty of ECM material (asterisk). ×2000.

protruded their leading filopodia through the fibrillar matrix network and could be observed forming specialized contacts with these structures (Figs 9 and 10). For the structural study of the ECM in the two embryos we used: (1) fixatives lacking cationic dyes to allow optimal examination of oriented collagen fibrils at the ultrastructural level (Löfberg *et al.* 1980); (2) fixatives containing ruthenium red to retract the whole proteoglycan molecules into granule-like structures without causing fragmentation of individual molecules (Hunziker and Schenk, 1987) or causing clustering of proteoglycans and affiliated molecules (as induced by CPC; Tuckett and Morriss-Kay, 1988), and minimizing masking of aligned collagen fibrils; and (3) PLP fixatives

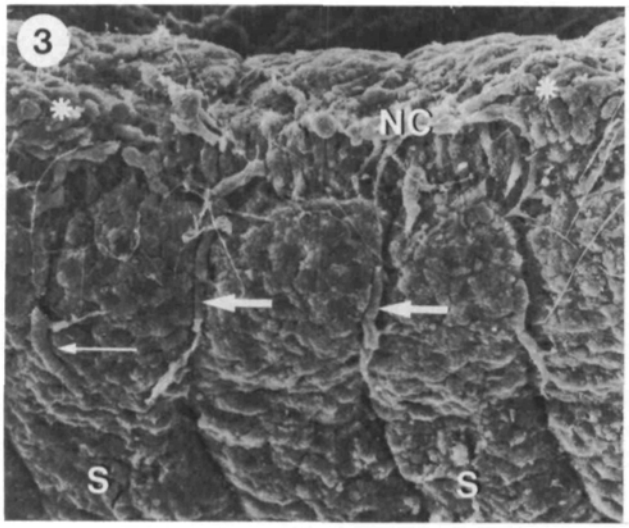


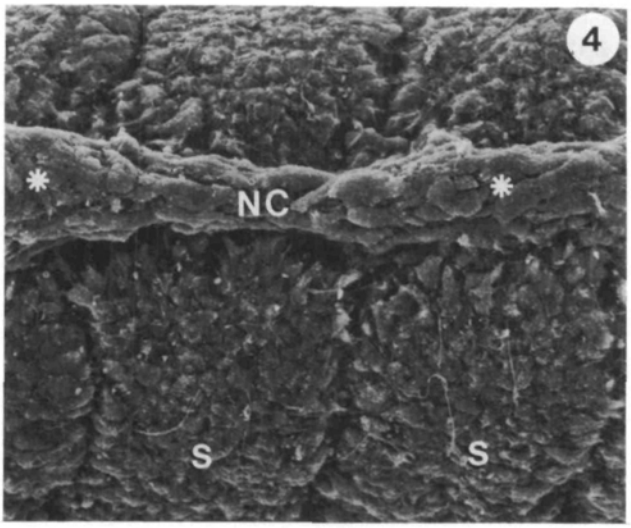


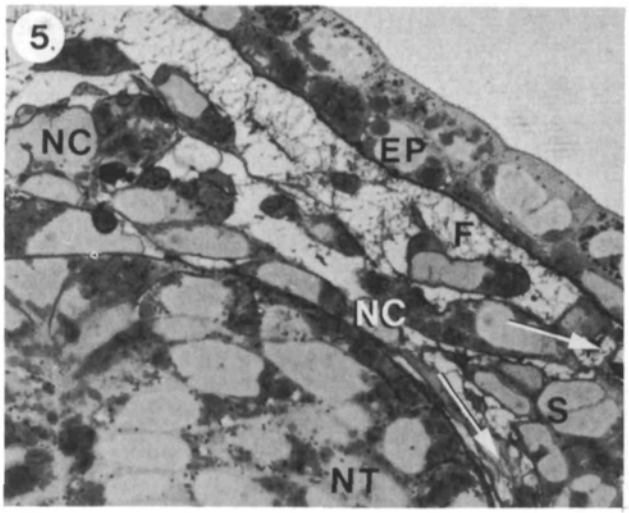


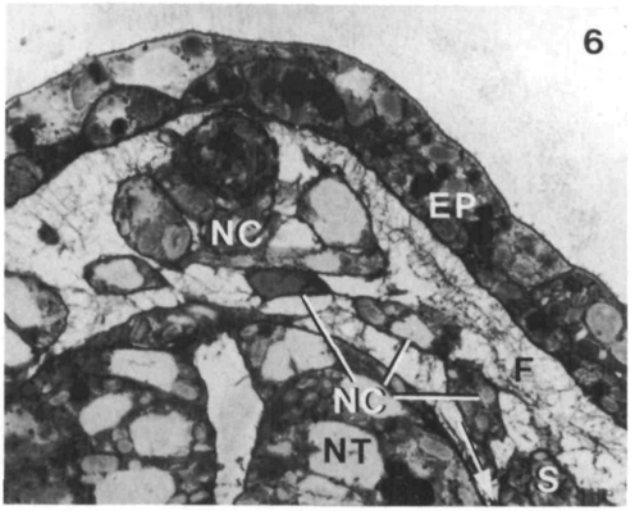


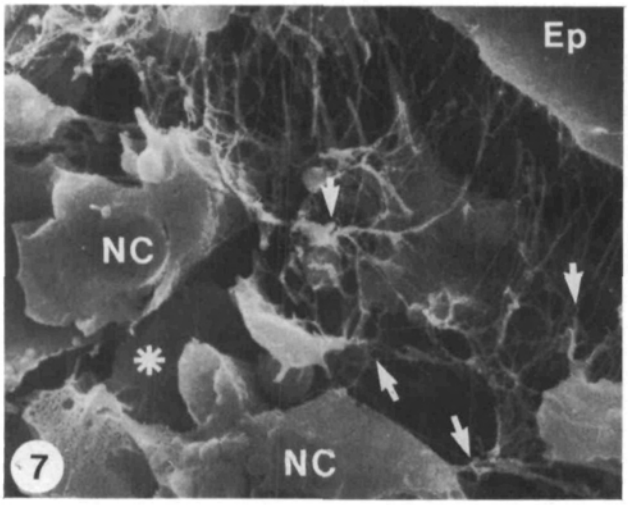


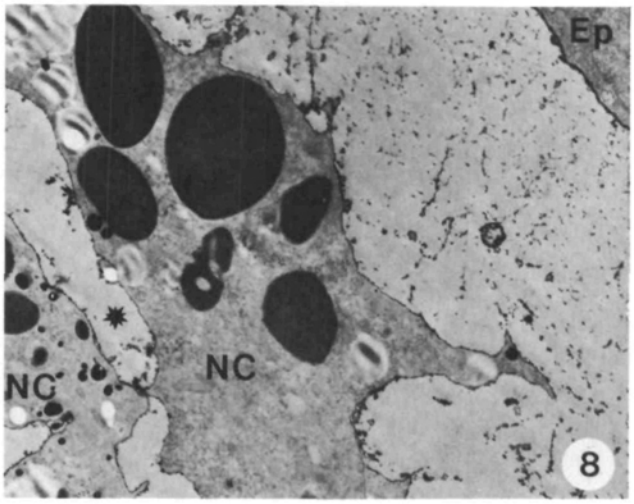

(McLean and Nakane, 1974) in combination with ruthenium red to enhance the retention of proteoglycans during tissue processing.

The general ultrastructural appearance of the interstitial ECM of dark and white embryos following ruthenium red/PLP–ruthenium red precipitation is illustrated in Figs 11 and 13. At stages of initial neural crest cell migration, the subepidermal and perineural basal laminae were continuous in both dark and white mutant embryos and local association of extracellular material indicated the progressive appearance of basement membranes-like structures. Typically, collagen-based fibrils oriented in arrays adjacent to the lamina densa (Fig. 12) from which they were separated by amorphous, flocculent material (Sanders, 1979; Martins-Green and Erickson, 1987; Inoue and Leblond,

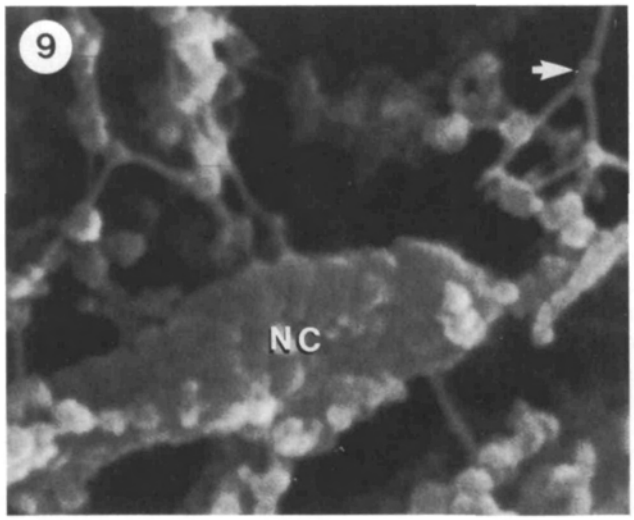


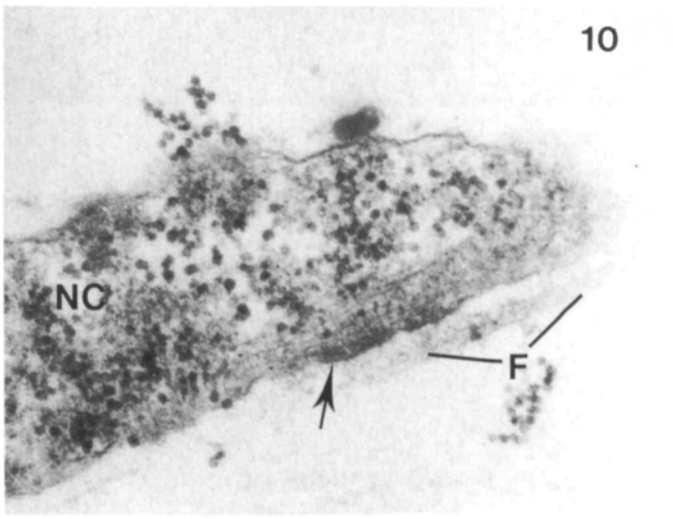


**Fig. 9.** High magnification SEM micrograph of a filopodium extended by a neural crest cell progressing through the subepidermal matrix network. Its surface, which appears granulated as a result of ruthenium red-precipitation of its associated extracellular components, seems to be in intimate contact with the ECM network. Arrow indicates a characteristic ungranulated microfibril with bifurcated arms linking to collagenous fibrils (compare with Fig. 14). ×30 000.

**Fig. 10.** TEM micrograph of a contact specialization, i. e. an electron-dense plaque on the cytoplasmic side of the plasma membrane (arrow), formed at the site of close cell–matrix contact. ×60 000.

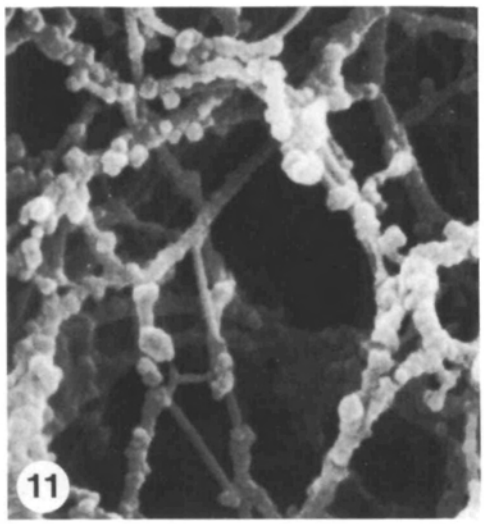


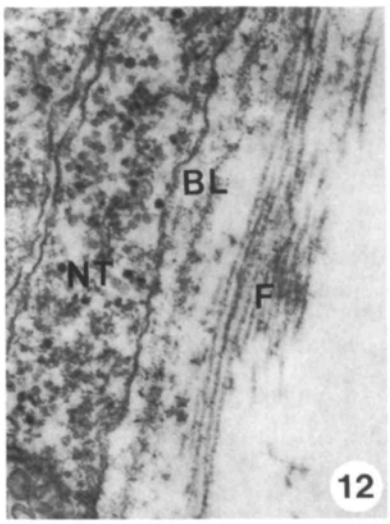



**Fig. 11.** High magnification SEM micrograph illustrating the intricate network arrangement of ECM fibrils along the medioventral neural crest migratory pathway. Virtually each fibril is decorated with ruthenium red-precipitated granules of different sizes. ×21 000.

**Fig. 12.** Basement membrane of the neural tube at initial stages of neural crest cell migration and as observed by TEM. Collagenous fibrils (F) can be seen oriented in the dorso-ventral direction. Note the contiguous basal lamina (BL) on the basal side of the epithelial neural tube cells (NT) and the amorphous material of the lamina apposing the array of collagen fibrils. ×68 000.

**Fig. 13.** High magnification TEM micrograph of an individual matrix fibril. The evident striation confirms its collagenous nature and the associated electron-dense granules illustrate retracted proteoglycans. ×200 000.

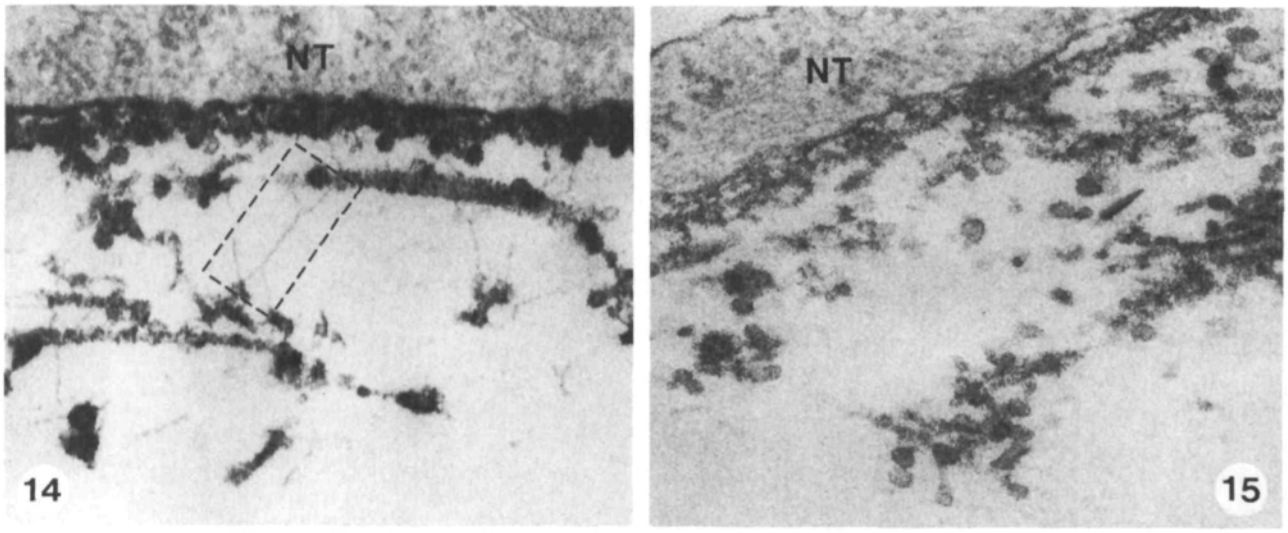


**Fig. 14.** TEM micrograph showing collagen fibrils and their associated granules of the neural tube (NT) basement membrane, following fixation in the presence of ruthenium red. Numerous 3–5 nm 'microfibrils' can be seen interconnecting the larger collagen fibrils to the basement membrane, occasionally *via* electron-dense granules. The area delineated illustrates a typical bifurcated microfibril. This particular specimen was incubated in buffer lacking enzyme and therefore represents a control to the enzyme-treated section shown in Fig. 15. ×33 000.

**Fig. 15.** The neural tube basement membrane in a region corresponding to that shown in Fig. 14, but following *Streptomyces* hyaluronidase digestion. Note the decrease in overall amount of ruthenium red-precipitated ECM material and the disappearance of the bifurcated microfibrils, indicating that these are composed of hyaluronan. Similar findings have also been reported in the chick embryo (Sanders, 1979). ×33 000.

1988). The basement membranes had a thicker appearance in the more dorsal regions of the embryo, indicating that development of complex basement membranes occurred in a dorsoventral succession. Numerous, 3–5 nm thick fibrils were observed anchored between cells/basement membranes and the collagenous interstitial matrix fibrils through branched arms (Figs 9, 11, 14, and 15). These fine fibrils had the morphological appearance of hyaluronate–proteoglycan complexes precipitated by (PLP)/ruthenium red (Scott, 1985; Turley *et al.* 1985; Hunziker and Schenk, 1987). Consistent with their morphology, these microfibrils were found to be susceptible to *Streptomyces* hyaluronidase digestion which degraded them and caused an overall reduction in ruthenium red-precipitated ECM material (see below).

*Structural divergencies of the white subepidermal ECM*

No differences could be disclosed morphologically between subepidermal basement membranes of dark and white mutant embryos, whereas interstitial matrices diverged in overall structure. The interstitial matrix fibrils suspended in the subepidermal spaces of both dark and white mutant larvae varied considerably in length and thickness, and appeared irregularly organized. Alignment of subepidermal matrix fibrils in the direction of cell movement was observed in both embryos in connection with neural crest cells migrating individually; probably as a result of traction by the moving cells. Although no overall difference in orientation of matrix fibrils deposited ahead of the moving neural crest cell front could be observed between dark and white matrices, a striking dissimilarity was detected in the amount of electron-dense granules that decorated individual matrix fibrils (Figs 16 and 17). To quantify this difference and determine whether it was significant, we carried out pairwise statistical examinations of the extent of granulation on interstitial matrix fibrils by employing computer-aided image processing and morphometry. The quotient of projected fibril area/fibril length of individual fibril segments analyzed by SEM was adopted to denote the degree of granulation. The median values of these quotients for fibrils of the regional matrices of the two embryos are summarized in Fig. 22. In pairwise comparisons (e.g. D/− subepidermal *versus* dd subepidermal ECM at stage 30 and 35), the morphometric analysis demonstrated that granulation was significantly lower ($P>0.001$ according to Mann-Whitney U-test) in the subepidermal ECM of white embryos at both initial and advanced stages of neural crest cell migration.

Generally, granules were present on virtually all fibrils, but were most dense on thick fibrils and scarce or absent from the finest fibrils. These latter fibrils did not exhibit collagenous characters. TEM examination of the granules attached to interstitial matrix fibrils, as well as decorating cell surfaces, showed that they were composed of clustered microspheres presumably corresponding to single proteoglycan molecules. The density of subepidermal matrix fibrils and their associated granules progressively decreased further down the flanks of both larvae, but remained particularly concentrated in the grooves formed at the intersomitic clefts. An abrupt diminution in the overall amount of inter-

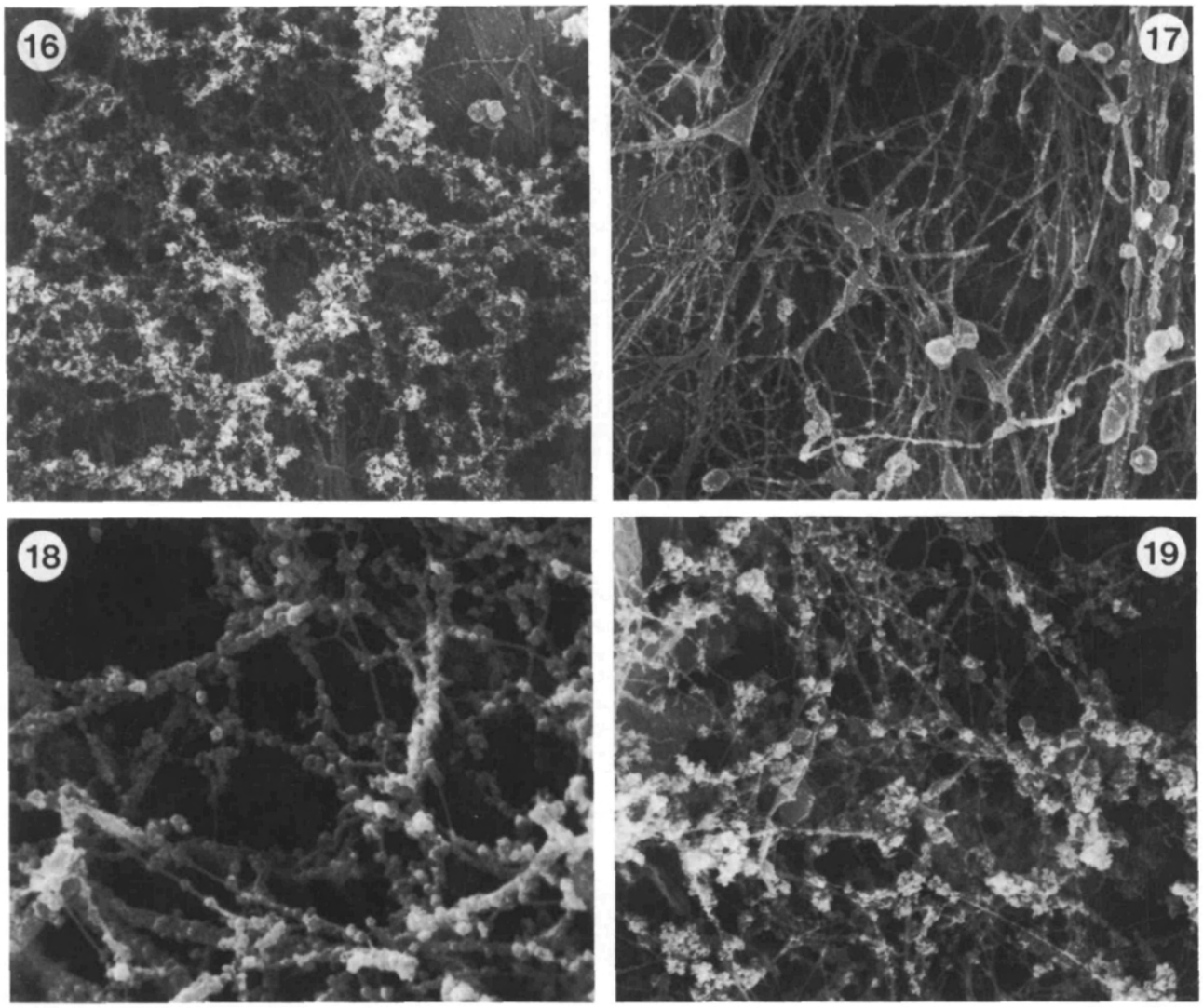


**Fig. 16.** SEM micrograph of the interstitial ECM in the subepidermal space of a dark embryo at initial neural crest cell migration. Local fixation of the ECM *in vivo* in the presence of ruthenium red retains a fibrillar network which appear copiously covered with proteoglycan granules. ×5300.
**Fig. 17.** A comparable subepidermal region as that shown in Fig. 16 but in a similarly fixed white mutant embryo. The subepidermal matrix fibrils of this embryo appear almost devoid of granules. ×5000.
**Fig. 18.** SEM micrograph showing the network assembly and extent of granulation of the ECM along the medioventral migratory pathway of a dark embryo, at initial neural crest cell migration. ×3000.
**Fig. 19.** Perineural ECM at initial neural crest cell migration in a white mutant embryo. The degree of granulation of the ECM fibrils in this region is virtually identical to that observed in the corresponding region of the dark embryo. ×5300.

stitial ECM occurred level with the endodermal tissue, which corresponds to the unpigmented portion of the larval body.

*Local restriction of the structural differences of the ECM as demonstrated by comparable appearance of perineural matrices*

On the dorsolateral aspect of the neural tube, well prior to neural crest cell migration, arrays of striated, 20–25 nm thick fibrils were oriented perpendicular to the neural axis. The alignment of the fibrils coincided with the putative migratory direction of neural crest cells (Löfberg *et al.* 1980). Moreover, the assembly and orientation of these fibrils, which was most evident in SEM specimens fixed in the absence of ruthenium red, was similar in dark and white mutant embryos and resembled that observed in the chick embryo (Allenspach and Clark, 1988; Newgreen, 1989). The fibrillar ECM suspended between neural tube and somites along the medioventral pathway displayed an identical network organization in embryos of both strains. Moreover, similarly to the subepidermal ECM, matrix fibrils of the perineural region showed a considerable variation in size and extent of granulation. The degree of granulation on matrix fibrils of the perineural matrix was comparable in dark and white mutant embryos (Figs 18 and 19). In both types of embryos at initial and advanced phases of neural crest

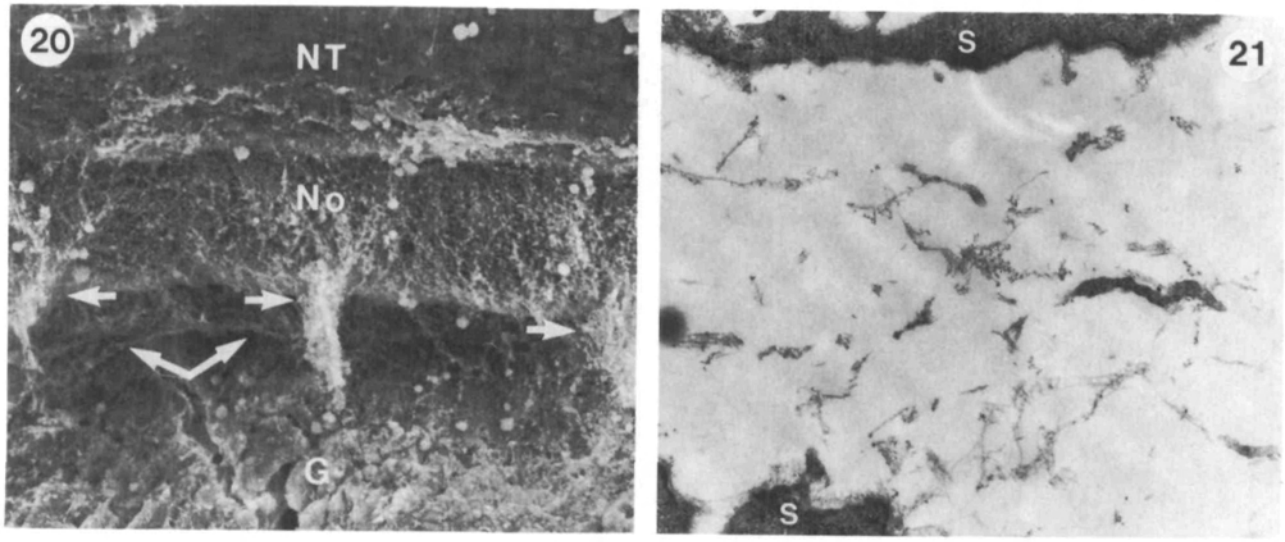


**Fig. 20.** SEM micrograph showing a lateral view of a selected axial region in a dark embryo in which several somite blocks have been removed. The recurrent tufts of congregated ECM fibrils seen on the lateral neural tube derive from the intersomitic cleft (single arrows). The fibrils of these tufts form a contiguous network that extends from the neural tube (NT)–notochord (No) complex to the epidermal basement membrane. Immediately below the notochord, strands of fibrillar material can also be seen connecting the intersomitic matrix tufts to the basement membrane of the notochord (double arrow). G=lateral surface of the presumptive gut wall. ×360.

**Fig. 21.** TEM micrograph of a horizontal section through an intersomitic cleft. The ECM shown in this micrograph corresponds to the tufts seen in Fig. 20 (S=somites). ×15000.

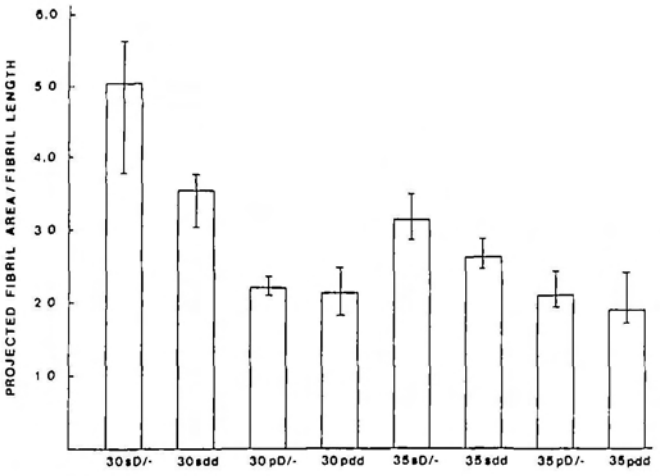


**Fig. 22.** Diagram summarizing the results of the morphometric analysis of the ECM in the two embryos. The median values for the ratio between projected fibril area and fibril length with 95% confidence limits (indicated by error bars) are given for subepidermal (s) and perineural (p) ECM in dark (D/−) and white (dd) embryos at stages of initial (30) and advanced (35) neural crest cell migration.

cell migration, the degree of granulation of the perineural matrix fibrils was lower than that of fibrils in the subepidermal region (Fig. 22). By removing selected somites from SEM specimens fixed in the presence of ruthenium red, it was possible to unfold tufts of ECM fibrils that were anchored to both the lateral neural tube surface and the subepidermal basement membrane, and that converged within the intersomitic clefts (Figs 20 and 21). The perineural basal laminae/basement membranes of the two embryos were morphologically indistinguishable, but the amount of material associated with the laminae was lower than that contiguous with the subepidermal laminae. The perinotochordal regions of both dark and white mutant embryos were filled with a dense and intricate fibrillar meshwork, which projected out radially from the notochordal capsule. The fibrils of this network were equivalently decorated with electron-dense granules in both embryos.

### *Structural changes in the matrix at phases of advanced neural crest cell migration*

At advanced stages of neural crest cell migration, the density of matrix fibrils increased along the migratory pathways of both dark and white mutant embryos. The greatest accretion of matrix fibrils occurred in the subepidermal spaces. In contrast, the amount and size of electron-dense granules decreased considerably in these regions, with the proportionally greatest decrease in dark embryos. The subepidermal basement membranes progressively increased in thickness and exhibited a continuous thick appearance in both dark and white mutant embryos. The perineural and perinotochordal basement membranes, however, maintained a broadly similar structure to that exhibited during initial neural crest cell migration. Similarly, the degree of granulation of the perineural ECM of the two embryos remained virtually constant (Fig. 22).

### *Immunolocalization of characterized ECM components*

To optimize comparison, immunohistochemical stainings with each antibody were carried out simultaneously

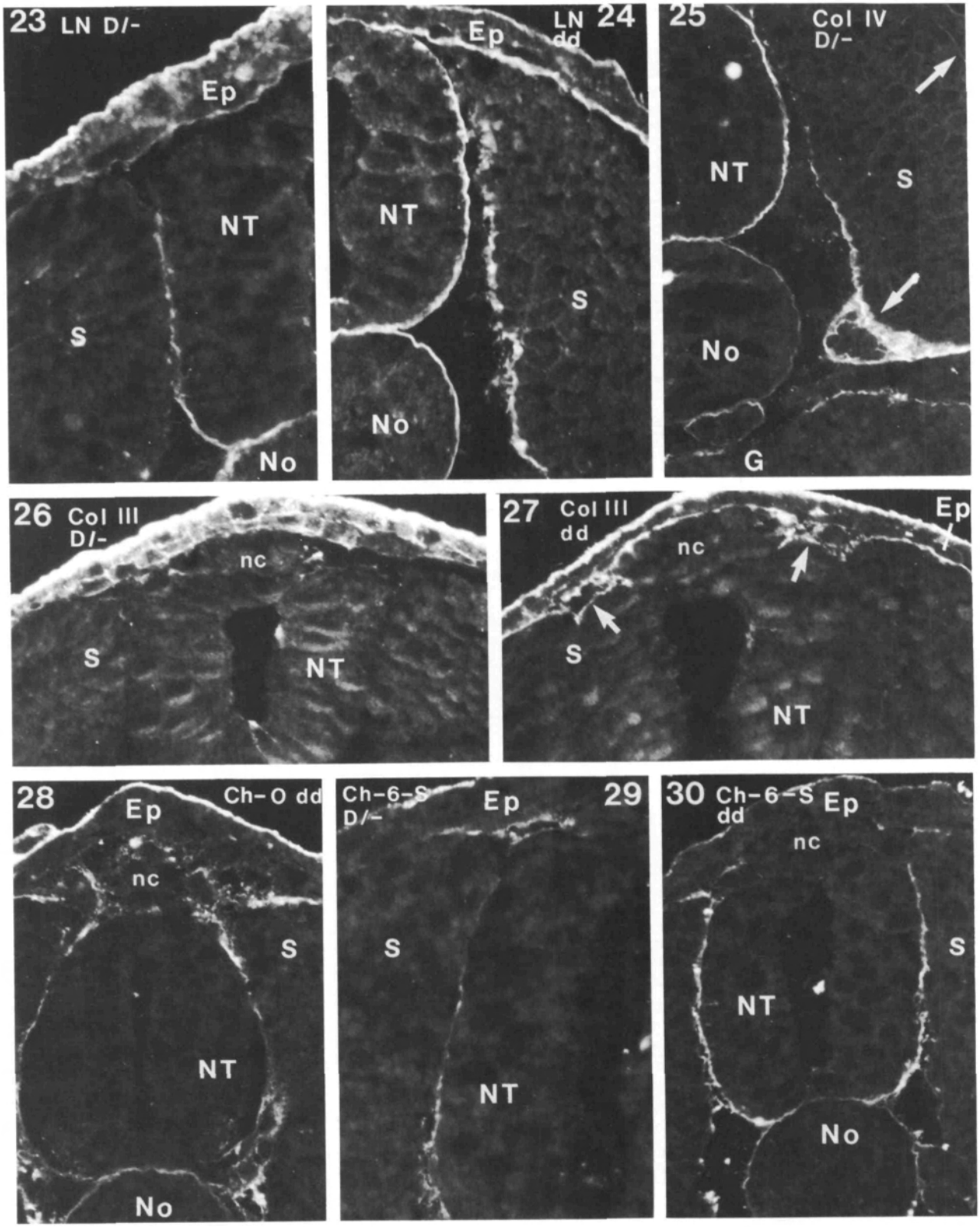


on adjacent sections from dark and white embryos. The immunohistochemical differences in the distribution of various matrix molecules are illustrated schematically in Fig. 39. Fibronectin, laminin, collagen types I and IV were all abundantly distributed in the ECM of the neural crest migratory pathways of dark and white mutant embryos (Figs 23–25, 31, and 34). At initial cell migration, both the subepidermal and medioventral migratory routes were strongly labelled in the two embryos. Labelling for fibronectin and collagen type I

**Figs 23–30.** Fluorescence micrographs showing representative stainings obtained after simultaneous antibody incubation of adjacent transverse sections from dark (D/−) and white mutant (dd) embryos at stages of initial neural crest cell migration.

**Fig. 23.** Laminin staining of dark embryos was confined to the basal portion of the epidermis (Ep), neural tube (NT) and notochord (No), but appears locally discontinuous along the dorsal portion of the subepidermal compartment and around the somites (S). ×120.

**Fig. 24.** The corresponding staining in the white mutant embryo coincides with that in dark embryos but was more uniform. ×120.

**Fig. 25.** Representative immunostaining for collagen type IV along the medioventral neural crest migratory pathway and a selected area of the subepidermal pathway in dark embryos. The subepidermal staining (*upper arrow*) was generally weaker than the corresponding around the neural tube. A portion of the sclerotome is brightly fluorescent (*lower arrow*). ×120.

**Figs 26 and 27.** Collagen type III labelling in dark and white mutant embryos, respectively. In the dark embryo, immunoreactivity for collagen type III was observed within the epidermis and along its dorsal basement membrane. In white mutant embryos the fluorescence within the epidermis was discontinuous, whereas staining was pronounced subepidermally and on the dorsolateral aspect of the neural tube (*arrows*). ×120.

**Fig. 28.** Immunostaining for the unsulfated chondroitin (CH-0) moiety of proteoglycans. Labelling was intense in the ECM of the subepidermal and medioventral migratory pathways of the neural crest, where it decorated various tissue structures as well as the interstitial matrix network. ×120.

**Figs 29 and 30.** Cross-sections from dark and white mutant embryos stained for the chondroitin-6-sulfate (Ch-6-S) determinant of proteoglycans. Staining was evident along both migratory pathways, but was more discontinuous in the dark embryo (29) than in the white embryo (30). ×120 and ×160.

was pronounced in the interstitial ECM between the epidermis and somites, and the perineural ECM suspended between somites and neural tube. Immunoreactivity for these molecules was also observed around the notochordal capsule and its associated fibrillar matrix, and on the lateral side of the sclerotome. Both matrix components were extensively immunolocalized in association with basement membranes and within the intersomitic clefts, whereas only fibronectin was detectable between premigratory neural crest cells. Labelling for fibronectin was equivalently strong in the intersomitic clefts, but was discontinuous on the dorsolateral somite surfaces of white mutant embryos. Immunostaining for collagen type I in white embryos differed from that in dark animals by being discontinuous along the neural tube basement membrane and lateral sclerotome.

Laminin and collagen type IV colocalized along basement membranes and were scarcely detectable in the interstitial matrices (Figs 29–31, and 34). The distribution patterns of these ECM molecules were broadly similar in dark and white mutant embryos, but some local differences could be observed. Immunolabelling for collagen type IV and laminin was more pronounced in white mutant embryos, in the intersomitic clefts and along the subepidermal basement membrane respectively.

Collagen type III was exclusively detected in the most dorsal portion of the subepidermal compartment of dark embryos (Fig. 26). In contrast, in white mutant embryos, collagen type III distributed uniformly along the entire basement membrane of the epidermis as well as around the premigratory neural crest cord, including the dorsolateral aspect of the neural tube (Fig. 27).

At advanced stages of neural crest cell migration, immunolabelling for fibronectin, and collagen types III and IV was virtually equivalent in the two embryos. In contrast, immunoreactivity for laminin was most accentuated on the lateral somite surfaces of white embryos, whereas collagen type I labelling was most intense around the neural tube and sclerotome of dark embryos.

Antibodies recognizing proteoglycans bearing predominantly unsulfated chondroitin chains stained primarily the perinotochordal region of dark embryos at stages corresponding to initial neural crest cell migration. In contrast, distribution of these proteoglycans in the white mutant embryo at equivalent developmental stages was more widespread (Fig. 28). In white embryos, immunoreactivity for proteoglycans rich in unsulfated chondroitin was sparsely distributed along the basal side of the epidermis and more prominently around the neural tube. The anti-chondroitin antibody also decorated the notochordal capsule and its associated fibrillar network. The intersomitic staining was similarly pronounced in the two embryos. At stages of advanced neural crest cell migration, staining for proteoglycans rich in unsulfated chondroitin chains demarcated the entire neural tube and notochord surfaces of dark embryos, and a discontinuous labelling was also discernible around and within the prospective sclerotome (Figs 37 and 38). In white mutant embryos of comparable stages, unsulfated chondroitin staining was more homogeneously distributed along both migratory pathways of neural crest cells; i. e. the subepidermal pathway was more strongly stained than in dark embryos.

At developmental stages corresponding to initial neural crest cell migration, the chondroitin-4-sulfate proteoglycan subunit was not immunohistochemically detectable in either normal dark or white mutant embryos. A dense perinotochordal staining for proteoglycans bearing this determinant appeared in both embryos first at later phases of neural crest cell migration, with the staining pattern being more irregular in the white mutant embryo.

The immunoreactive pattern of proteoglycans rich in chondroitin-6-sulfate differed in dark and white mutant embryos in a fashion similar to that of proteoglycans with unsulfated chondroitin (Figs 29 and 30). At initial phases of cell movement in dark embryos, chondroitin-6-sulfate-bearing proteoglycans traced discontinuously the basement membrane of the epidermis as well as the perineural and perinotochordal regions, and were spar-

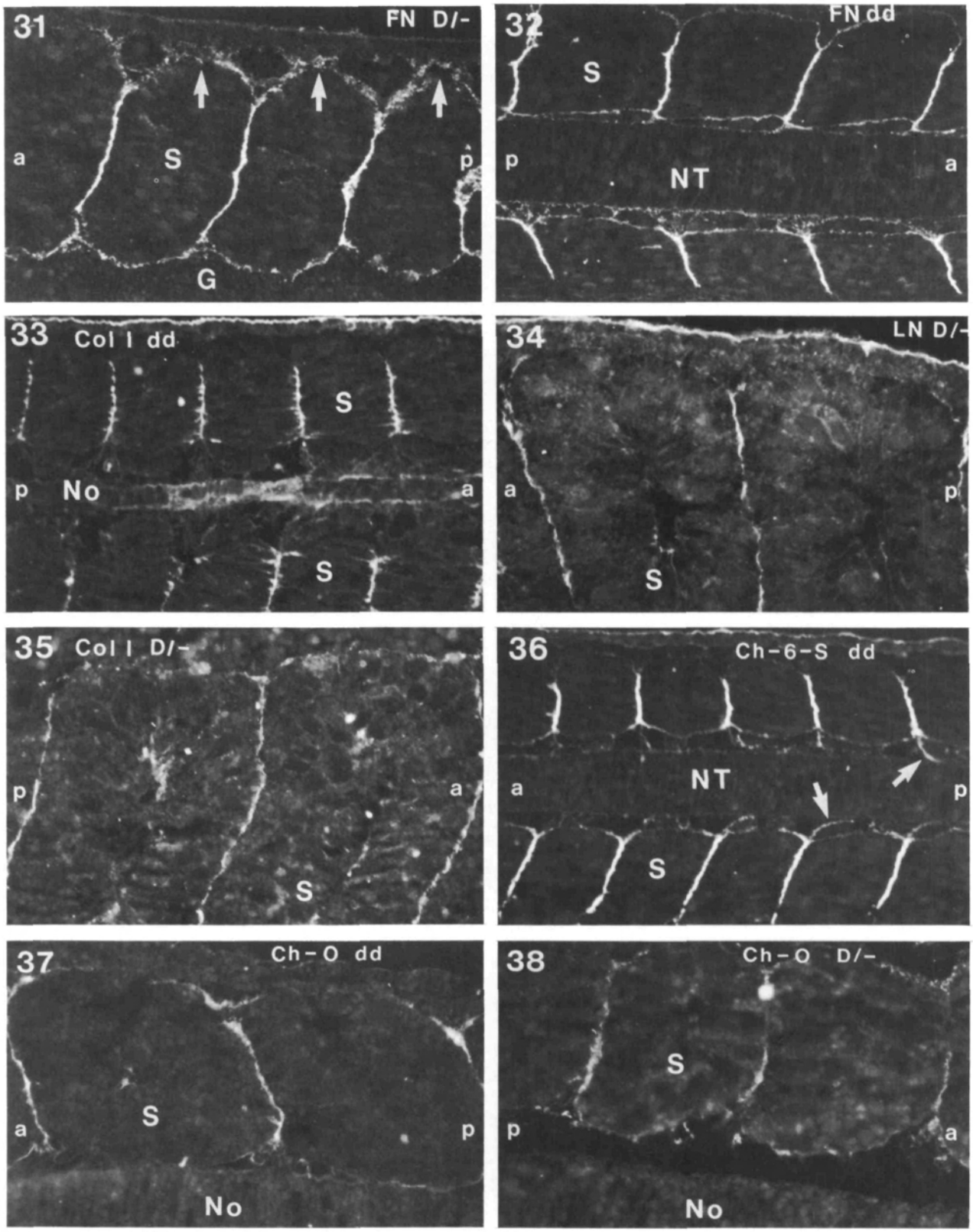


sely distributed around and within the somites (Fig. 29). Conversely, in white embryos a uniform staining was observed along both migratory routes of neural crest cells, including the intersomitic clefts (Fig. 30). Later in development, immunolabelling in the dark embryo was regionally comparable to that observed in white mutant embryos, with the exception of the dorsolateral aspect of the somites which was more prominently stained in the white mutant embryo. Staining for chondroitin-6-sulfate-rich proteoglycans

**Figs 31–38.** Fluorescence micrographs illustrating immunolabellings of longitudinal sections from dark and white mutant embryos at developmental stages corresponding to initial and advanced neural crest cell dispersion. In Figs 31, 34, and 37 the anterior portion of the embryo is to the left in the micrograph, whereas orientation is opposite in all other cases.

**Fig. 31.** Fibronectin labelling of somites (S) and their associated interstitial matrix in a dark embryo sectioned sagittally at initial neural crest cell migration. Arrows indicate immunoreactive fibrils anchored between the apical edge of the somites and the subepidermal basement membrane. Note also that the entire somite blocks are stained ×75.

**Fig. 32.** Fibronectin staining of a horizontal section through a white mutant embryo at stages of advanced neural crest cell migration. Staining surrounds the entire somite blocks but is considerably weaker on the dorsolateral surface facing the subepidermal space. ×70.

**Fig. 33.** Immunolabelling for collagen type I in a white mutant embryo sectioned horizontally at level of the ventral notochord (No). Note that staining in the intersomitic clefts extends into the intercellular spaces between prospective myotubes and that no staining can be observed on the dorsolateral aspect of the somite blocks. ×70.

**Fig. 34.** Intersomitic staining for laminin in a dark embryo sectioned sagittally at stages of initial neural crest cell migration. In horizontal sections it could also be noted that laminin immunoreactivity permeated the somites in a similar fashion as that observed for collagen type I. ×180.

**Fig. 35.** Staining for collagen type I in a similar sagittal section as shown in Fig. 34. The two molecules largely colocalize and show similar staining intensities. ×200.

**Fig. 36.** Staining for chondroitin-6-sulfate-bearing proteoglycans at advanced neural crest cell migration in a white mutant embryo. Labelling was dense in the intersomitic clefts and around the coalesced dorsal root ganglia (*arrows*). Immunoreactivity for proteoglycans rich in chondroitin-6-sulfate coincided with that of their ligand collagen type I. ×70.

**Figs 37 and 38.** Oblique sagittal sections through white mutant and dark embryos, respectively, stained at stages of initial neural crest cell migration with an antibody recognizing unsulfated chondroitin chains of proteoglycans. Immunoreactivity for this proteoglycan determinant was more pronounced in the white embryo and overall was weaker than that for chondroitin-6-sulfate. ×140 and ×130.

was accentuated in the subepidermal space and intersomitically (Fig. 36), particularly in dark embryos, and around the periodic pigment cell aggregates that formed along the premigratory neural crest cord (Epperlein and Löfberg, 1984). In spaces between these aggregates, staining appeared patchy around the few neural crest cells still in their premigratory position.

Keratan sulfate-bearing proteoglycans were solely immunolocalized along the medioventral migratory pathway of the neural crest, and in analogous distributions in the two embryos. At initial neural crest cell movement, the staining on the lateral surface of the neural tube appeared more homogeneous in white mutant embryo than in the dark. At later developmental stages, however, immunostaining for keratan sulfate was identical in both types of embryo.

*Biochemical analysis of ECM explanted on membrane microcarriers*

Utilizing membrane microcarriers, region-specific ECMs were adsorbed *in vivo* from neural crest migratory pathways of dark and white mutant embryos (Löfberg *et al.* 1985; Perris and Löfberg, 1986). Subsequent electrophoretic micro-analyses were restricted to ECM isolated from embryos at initial stages of neural crest cell migration (stages 30–31). Although a fully representative repertoire of ECM macromolecules cannot be expected to be retained on microcarriers, the technique offers the advantage of isolating regional ECMs synthesized and secreted in the proper location in the embryo. Ten to fifteen ECM-covered microcarriers were found to provide enough material for each electrophoretic analysis. A total of seven one-dimensional separations of ECM samples analyzed in parallel according to this procedure revealed only a minor compositional difference between the subepidermal and perineural ECMs of the two embryos. This consisted in a broad (subepidermal) *versus* narrow band (perineural) at about 55–60 000 $M_r$ (data not shown). Extraction of the matrix samples with Triton X-100 largely prevented this smearing but in addition eliminated several bands appearing without Triton X-100 extraction. Extraction with other detergents had similar effects.

Two-dimensional electrophoretic separation (5 cases) of subepidermal and perineural ECMs disclosed several differences. These consisted in the appearance of seven faint spots in gels of the dark subepidermal ECM in the molecular weight region corresponding to 30–60 000 $M_r$, which were absent in the corresponding molecular weight region of gels of the white mutant subepidermal ECM (Fig. 40). Gels from white mutant subepidermal ECM, on the other hand, showed a distinct spot at about 40 000 not contained by the parallel gel of dark subepidermal ECM. In addition, two prominent spots appeared exclusively in the white subepidermal ECM in the 130 000 region.

The protein patterns obtained after parallel, two-dimensional separation of perineural ECMs of dark and white mutant embryos were slightly different from each other and clearly distinguishable from the corresponding ones of the subepidermal ECMs (Fig. 40). The major differences occurred in the molecular weight region corresponding to 40–70 000. A conspicuous difference consisted in the appearance of a eight-spot row, which localized at about 50–55 000 in the white mutant perineural ECM, and which was not present in the parallel gels of dark perineural ECM. Two single spots were detectable at about 90 000 and 120 000 in the white perineural ECM, but not in the matching matrix of the normal dark embryo.

## Discussion

Several previous studies have suggested that the topographical organization of ECM substructures may determine the permissiveness of the matrix as a substrate

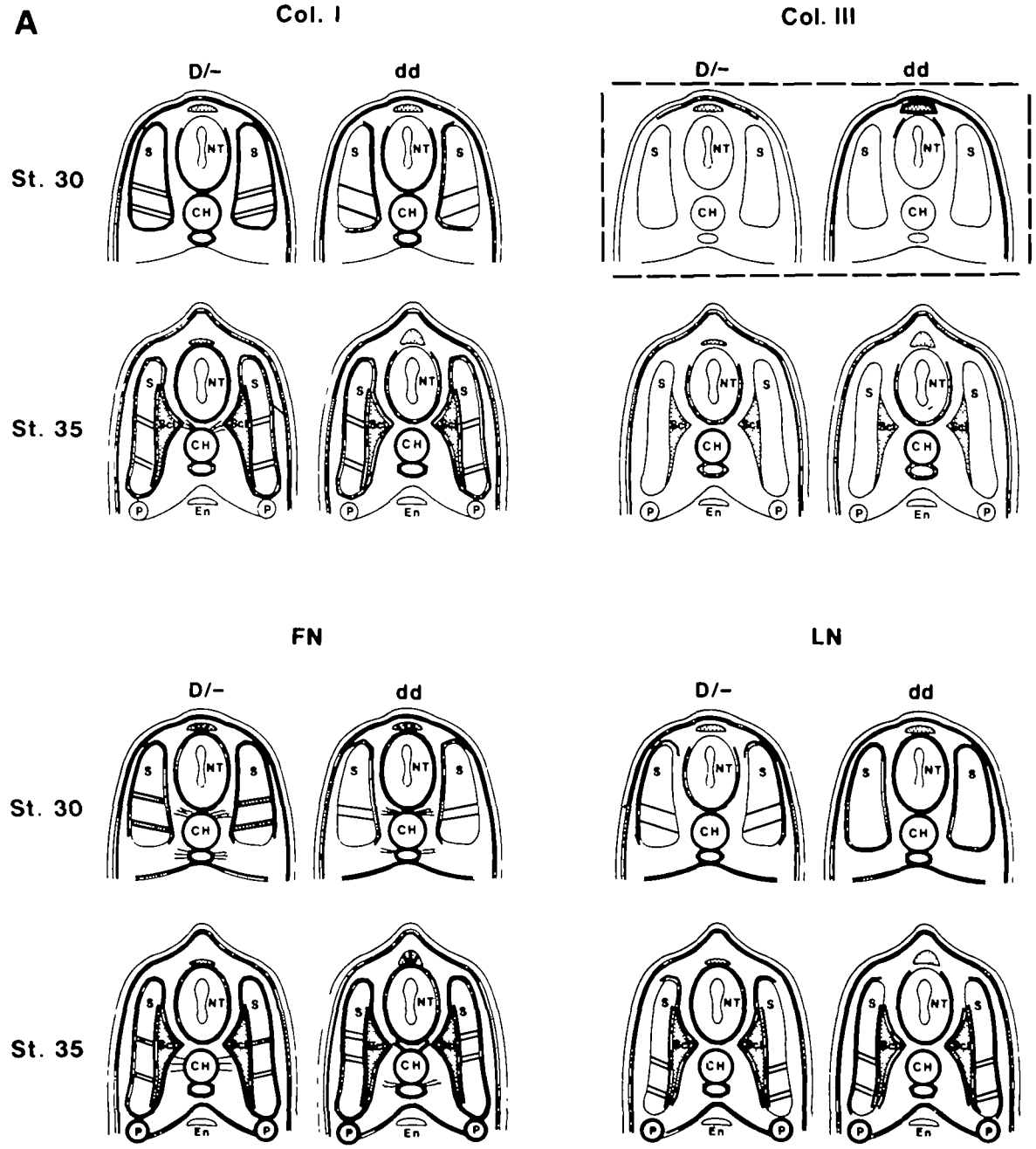


**Fig. 39.** A,B. Diagram summarizing the immunohistochemical staining patterns observed with (a) affinity purified antisera to collagen type I (Col I), collagen type III (Col III), fibronectin (FN) and laminin (LN), and (b) monoclonal antibodies recognizing proteoglycans rich in unsulfated chondroitin (Ch-O), chondroitin-4-sulfate (Ch-4-S), chondroitin-6-sulfate (Ch-6-S) and keratan sulfate (KS). Boxed section pairs denote the most conspicuous differences in staining pattern observed between dark and white embryos. Dense and weak immunoreactivity within the somites is indicated with double and single lines respectively. NT=neural tube; S=somites; CH=notochord; Scl=sclerotome; En=endoderm; P=pronephric ducts. The premigratory neural crest cord is illustrated as a dotted irregular circle on top of the neural tube.

for neural crest cell migration (Ebendal, 1977; Löfberg *et al.* 1980; Allenspach and Clark, 1988; Brauer and Markwald, 1988; Newgreen, 1989). On the basis of this suggestion it could be assumed that the inhibited subepidermal neural crest cell migration in embryos of the white axolotl mutant could be attributed to a transiently defective topological arrangement of its subepidermal ECM. To some extent our present ultrastructural observations contradict this assumption by indicating that the matrix along the migratory pathways of neural crest cells of dark and white mutant embryos exhibits an indistinguishable configurational arrangement. These observations led us to the alternative hypothesis that the defect in the subepidermal ECM of

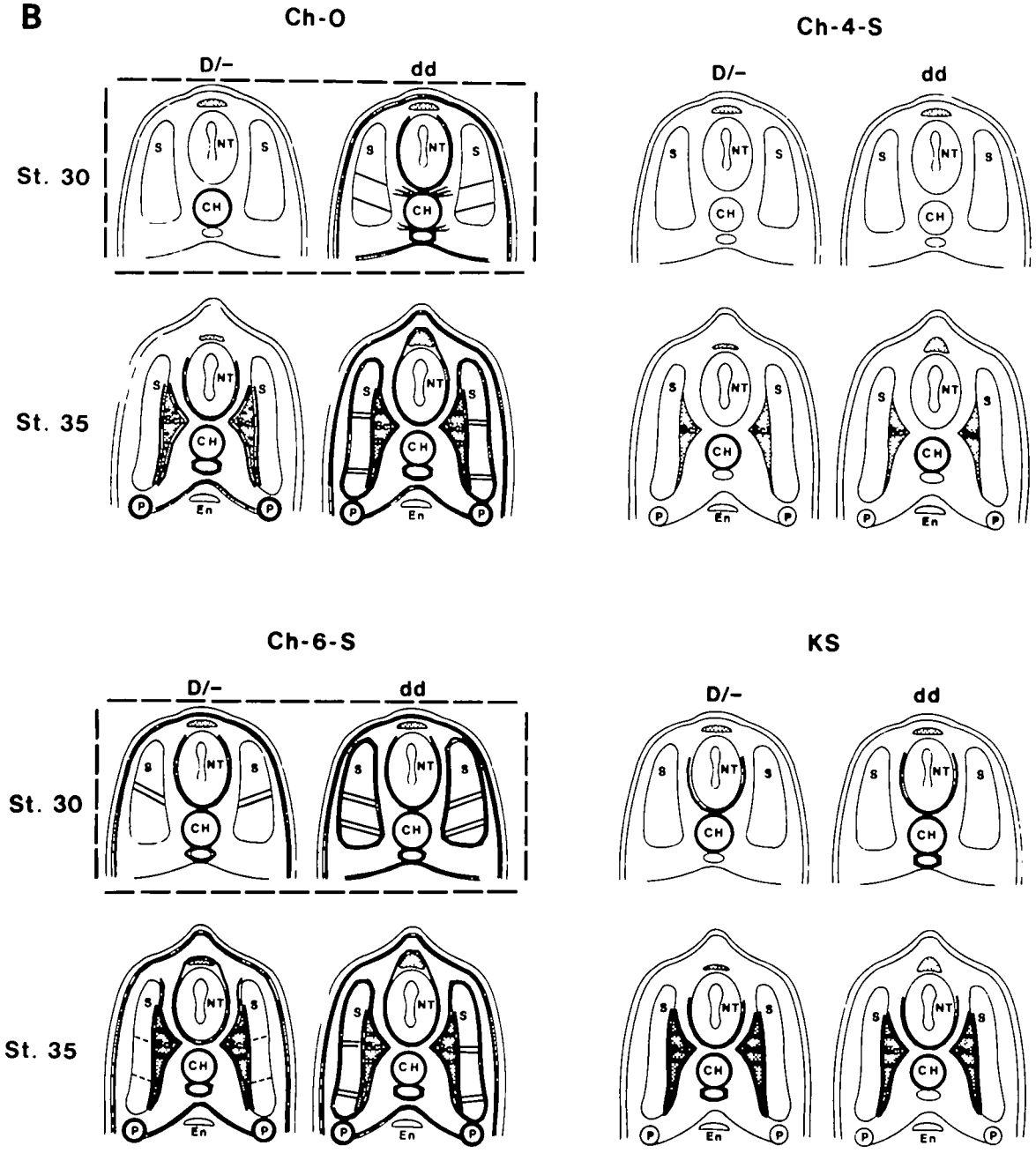


the white mutant embryo was more complex than simply an altered assembly of a constitutionally normal matrix.

We have previously correlated an increase in number of ECM fibrils surrounding the premigratory neural crest with initiation of cell movement (Löfberg *et al.* 1980; 1985). However, accumulation of extracellular material does not always imply a more favorable environment for cell migration since, for example, abundance of ECM in other embryonic areas seems to obstruct neural crest cell movement (Newgreen *et al.* 1986; Payette *et al.* 1988; Perris *et al.* 1990). In accordance with these observations is our finding that the dense perinotochordal ECM of both dark and white mutant axolotl embryos is avoided by the migrating neural crest cells. Local matrix density can probably influence the arrest of migrating neural crest cells as indicated by the occurrence of tightly packed fibril bundles on the lateral neural tube surface in the salamander *Hynobius*, which seem to correspond to sites of coalescence of the dorsal root ganglia (Hirano and Shirai, 1986). The present ultrastructural studies and recent immunohistochemical findings in the chick (Perris *et al.* 1989*b*) corroborate these observations and suggest that these fibrils attached to the neural tube at the level of the intersomitic septa are collagenous and are linked by hyaluronan–proteoglycans complexes.

The immunohistochemical data obtained in this study indicate that the distribution of fibronectin, laminin, collagen types I and IV, and proteoglycans bearing

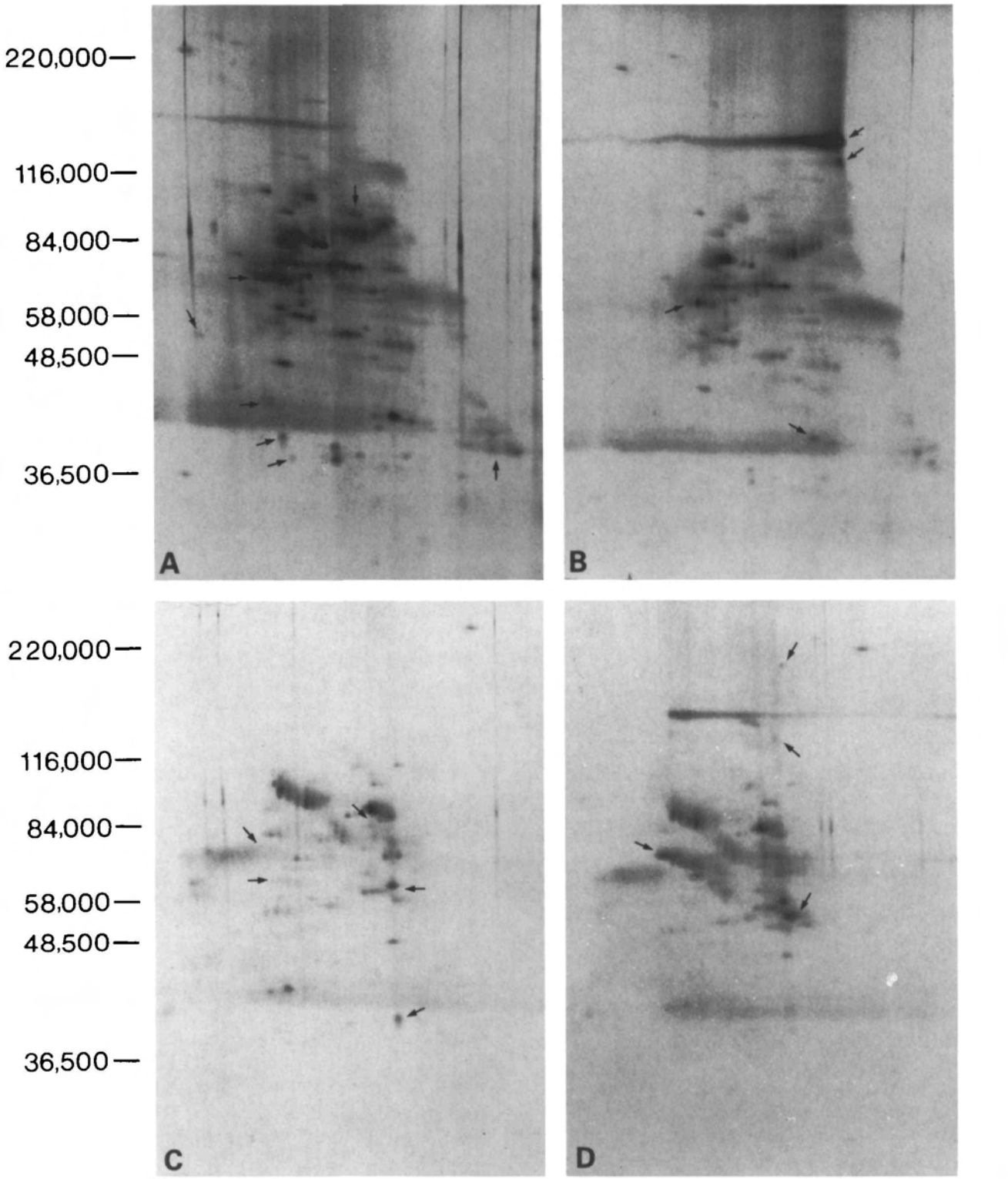


**Fig. 40.** A–D. Two-dimensional gel electrophoresis of ECMs adsorbed *in vivo* and explanted on membrane microcarriers from the subepidermal (A,B) and perineural (C,D) neural crest migratory pathways of dark (D/−) and white mutant (d/d) embryos. Optimal solubilization for this sensitive gel electrophoretic procedure does not include the complete repertoire of ECM proteins of the largest molecular masses, which presumably even after enzymatic predigestions would fail to enter the microthin 7.5% gels. Major differences in the electrophoretic pattern of the different regional ECMs of dark and white mutant embryos are indicated by the arrows. Molecular weight standards are indicated at the left.

predominantly chondroitin-4-sulfate and keratan sulfate side chains differs marginally in the ECM of dark and white mutant embryos. Some of the minor immunohistochemical differences in the distribution pattern of fibronectin and laminin could readily be due to differential masking effects. On the other hand, masking of immunogenic epitopes could reflect specific complexing and comformations of these molecules that prevent the occurrence of proper cell–matrix interactions during migration. In fact, there is *in vivo* evidence that neural crest cells require unrestricted access to extracellular fibronectin and to laminin complexed with heparan sulfate proteoglycan in order to accomplish their normal migration through the embryo (Boucaut *et al.* 1984; Bronner-Fraser, 1986; Bronner-Fraser and Lallier, 1988).

Although fibril density/arrangement was indistinguishable, a striking difference between the subepidermal ECMs of the two embryos was manifested by a significantly higher accumulation of electron-dense granules on the collagen fibrils of normal dark embryos. A similar difference in size and density of spherical elements associated with interstitial matrix fibrils has been described elsewhere (Spieth and Keller, 1984). In this previous investigation, however, the detergent cetylpyrinidium chloride was included in the fixative, and both cell membrane components (Tuckett and Morriss-Kay, 1988) and interstitial matrix structures were collapsed into heterogeneous spherical aggregates. These aggregates are presumed to embody the hyaluronan microfibrils, which we suggest here to function structurally as multiple linkages between cells/interstitial collagen fibrils and the basement membranes, and to comprise clusters of proteoglycans and affiliated molecules. Thus, this fixation protocol is particularly suitable for retention of hyaluronan in tissues (Derby and Pintar, 1978; Perris *et al.* 1990) but is inadequate when examining the detailed structure of the ECM (Hunziker and Schenk, 1987).

Ruthenium red-containing and PLP fixatives can be used to stabilize matrix complexes including hyaluronan, proteoglycan-like molecules and highly glycosylated proteins during tissue processing. After such structural preservation of the ECM, proteoglycan monomers retract to form electron-dense granules, the size of which largely corresponds to the size of the core protein and/or the glycosaminoglycan/protein ratio (Scott, 1985; Turley *et al.* 1985; Cidadao & David-Ferreira, 1986; Hunziker and Schenk, 1987). Ruthenium red and PLP may also bind to a variety of negatively charged molecules by nonspecific ionic interaction. The more pronounced distribution of electron-dense granules in the subepidermal ECM of the dark embryo could indicate that larger numbers of proteoglycan-like molecules are deposited in the dark subepidermal ECM. Alternatively, the same numbers of proteoglycan molecules could be present in the two embryos, but the relative size and protein/glycosaminoglycan ratio or the structure of the glycosaminoglycan moieties could differ. Furthermore, the difference in granulation could also reflect a discrepancy in the relative proportion of hyaluronan and proteoglycan-like molecules able to interact with hyaluronan, as well as a differential occurrence of link proteins causing destabilization of the complexes stained by the cationic dyes.

Our biochemical data suggest that several uncharacterized, highly glycosylated proteins, some of which are probably contained in the ruthenium red/PLP-precipitated granules, occur differentially distributed in dark and white subepidermal matrices. In addition, immunohistochemistry revealed that proteoglycan subsets bearing predominantly low sulfated and/or chondroitin-6-sulfate side chains were more abundantly distributed in the subepidermal ECM of the white mutant embryo. The implication of the predominant distribution of these proteoglycan types in the white mutant embryo is highlighted by parallel studies on the effects of these proteoglycans on neural crest cell migration. For instance, chondroitin sulfate proteoglycans derived from cartilage are nonpermissive substrates for chick neural crest cell–substrate adhesion (Newgreen, 1982), quail neural crest cell migration (Tan *et al.* 1987; Perris *et al.* in preparation), and axolotl neural crest cells migration *in vitro* (Perris and Johansson, 1987). In addition, this class of proteoglycans has been found to inhibit migration of neural crest cells over fibronectin, vitronectin, laminin and substrates of various types of collagens by a mechanism mediated by cell surface hyaluronan (Perris and Johansson, 1987; 1990). Finally, studies in *Taricha torosa* embryos have pointed out the importance of chondroitin sulfate proteoglycans in pigment cell patterning (Tucker, 1986; Tucker and Erickson, 1986).

Collagens are generally weak supporters of axolotl neural crest cell migration *in vitro*, and in particular collagen type III has been found to be poorly permissive for neural crest cell movement (Perris and Johansson, 1990; Perris *et al.* in preparation). In the light of these experimental data, it could be assumed that the extensive incorporation of collagen type III into interstitial fibrils of the white mutant embryo's ECM could be a relevant factor for the restriction of neural crest cell migration.

That the structural/compositional anomaly of the white ECM is local for the subepidermal space was further evidenced morphologically by the fact that the ECM deposited along the medioventral pathways (where neural crest cell migration appears normal) showed equivalent morphology in the two embryos. Interestingly, however, the perineural ECM of both embryos was less granulated than the subepidermal ECM of the white mutant embryo and the dark subepidermal ECM showed the overall highest granulation. Both immunohistochemistry and gel electrophoretic analysis of the perineural ECM of the two embryos disclosed additional molecular differences. The significance of the dissimilarities in structural and molecular composition of the equivalently migration-permissive subepidermal and perineural ECMs of dark embryos, and differences between the perineural ECMs of the dark and white mutant embryos remain unclear.

Several spatiotemporal changes in morphology and composition of the ECM along the neural crest migratory pathways of the two embryos seem to occur during the course of migration. For instance, in the subepidermal ECM, there is an obvious increase in fibril density dorso-ventrally, whereas the overall extent of granulation decreases. In contrast, the perineural ECM maintains broadly the same spatial organization in both embryos. Intriguingly, the perineural ECMs, at both initial and advanced stages of neural crest cell migration, and the subepidermal ECMs at stages of advanced migration markedly deviate ultrastructurally from that of the dark embryo at stages of initial migration, but possess an 'equivalent' ability to trigger the onset of neural crest cell migration (Löfberg *et al.* 1989*b*). The differential distribution of characterized matrix components, including laminin, collagen types I/III, and proteoglycans bearing predominantly unsulfated and chondroitin-6-sulfate side chains adds to the series of changes that occur during the course of neural crest cell migration, and that preserve compositional differences in regional matrices of the two embryos, which are independent of their ability to support neural crest cell migration.

Finally, we conclude that the inability of the white subepidermal ECM to function as a substrate for neural crest cell migration (Spieth and Keller, 1984; Löfberg *et al.* 1989*a*,*b*) cannot solely be attributable to an anomaly in spatial organization since qualitative as well as quantitative differences in its structural/molecular composition are expressed at stages of initial neural crest cell migration. The divergent composition of the white subepidermal ECM appears to involve differential distribution of characterized matrix components and differential occurrence of a variety of uncharacterized molecules. We suggest that these differences may cooperatively determine its assembly and the proper modelling of a migration-permissive environment.

We wish to express our gratitude to Drs Jean-Claude Boucaut, Richard Hynes, Antti Vaheri, Daniel Hartmann, Charles Little, Jörgen Wieslander, Brigid Hogan and Bruce Caterson for the generous supply of antibodies. We thank Vibeke Nilsson, Lars-Erik Jönsson and Henrik Olsson for technical assistance, and Dr Marianne Bronner-Fraser for critical reading of the manuscript and financial support during the final phases of the work. The study was sponsored by the Swedish Natural Science Research Council (grant B-BU 3810-104).

## References

Allenspach, A. L. and Clark, P. J. (1988). Retention and structure of extracellular matrix in early chick embryos after quick-freezing and freeze-substitution. *Eur. J. Cell Biol.* **46**, 531–538.

Bogomolova, V. I. and Korochkin, L. I. (1973). Development of pigmentation after transplantation of presumptive epidermis between embryos of white axolotl Ambystoma mexicanum of different ages. *Ontogenez* **4**, 420–424.

Borack, L. I. (1972). Gene action on proliferation and migration in the developing neural crest in black and white axolotl, Ambystoma mexicanum, Shaw. *J. exp. Zool.* **179**, 289–298.

Bordzilovskaya, N. P. and Dettlaff, T. A. (1979). Table of stages of the normal development of axolotl embryos and the prognostication of timing of successive developmental stages at various temperatures. *Axolotl Newslett.* **7**, 2–22.

Boucaut, J-C., Darribere, T., Poole, T. J., Aoiyama, H., Yamada, K. M. and Thiery, J.-P. (1984). Biologically active synthetic peptides as probes of embryonic development: A competitive peptide inhibition of fibronectin function inhibits gastrulation in amphibian embryos and neural crest cell migration in avian embryos. *J. Cell Biol.* **99**, 1822–1830.

Brauer, P. R. and Markwald, R. R. (1988). Specific configurations of fibronectin-containing particles correlates with pathways taken by neural crest cells at two axial levels. *Anat. Rec.* **222**, 69–82.

Bronner-Fraser, M. (1986). An antibody to a receptor for fibronectin and laminin perturbs cranial neural crest development *in vivo*. *Devl Biol.* **117**, 528–536.

Bronner-Fraser, M. and Lallier, T. (1988). A monoclonal antibody against a laminin-heparan sulfate proteoglycan complex perturbs cranial neural crest migration *in vivo*. *J. Cell Biol.* **106**, 1321–1329.

Caterson, B., Calabro, T. and Hampton, A. (1987). Monoclonal antibodies as probes for elucidating proteoglycan structure and function. In *Biology of Proteoglycans* (eds T. N. Wight, and R. P. Mecham), pp. 1–25. London, Academic Press Inc.

Cidadao, A. J. and David-Ferreira, J. F. (1986). A method for TEM visualization of the extracellular matrix three-dimensional organization in tissues. *J. Microsc.* **142**, 49–62.

Dalton, H. C. (1950). Inhibition of chromatoblast migration as a factor in the development of genetic differences in pigmentation in white and black axolotl. *J. exp. Zool.* **115**, 151–173.

Derby, M. A. and Pintar, J. E. (1978). The histochemical specificity of Streptomyces hyaluronidase and chondroitinase ABC. *Histochem. J.* **10**, 529–547.

Dufour, S., Duband, J.-L. and Thiery, J.-P. (1987). Role of the major cell-substratum adhesion system in cell behavior and morphogenesis. *Biol. Cell* **58**, 1–14.

Ebendal, T. (1977). Extracellular matrix fibrils and cell contacts in the chick embryo. The possible roles in orientation of cell migration and axon extension. *Cell Tissue Res.* **175**, 439–458.

Epperlein, H. H. and Löfberg, J. (1984). Xanthophores in chromatophore groups of the premigratory neural crest initiate the pigment pattern of the axolotl larva. *Wilhelm Roux' Arch. devl Biol.* **193**, 357–369.

Epperlein, H. H., Perris, R. and Löfberg, J. (1986). Environmental control in pigment pattern formation of the axolotl larva. In *Progress in Biological and Clinical Research* (H. C. Slavkin, ed.), vol. 217B, pp. 191–194. New York: A. R. Liss.

Frost, S. K. and Malacinski, G. M. (1980). The developmental genetics of pigment mutants in the Mexican axolotl. *Dev. Genet.* **1**, 271–294.

Hirano, S. and Shirai, T. (1986). Scanning electron microscopic observations on the early development of the spinal ganglia in salamander larvae. *Okajimas Folia Anat. Jap.* **62**, 385–398.

Hunziker, E. B. and Schenk, R. K. (1987). Structural organization of proteoglycans in cartilage. In *Biology of Proteoglycans* (eds T. N. Wight, and R. P. Mecham), pp. 155–185. London, Academic Press Inc.

Inoue, S. and Leblond, C. P. (1988). Three-dimensional network of cords: The main component of basement membranes. *Am. J. Anat.* **181**, 341–358.

Keller, R. E., Löfberg, J. and Spieth, J. (1982). Neural crest cell behavior in white and dark embryos of Ambystoma mexicanum: Epidermal inhibition of migration in the white axolotl. *Devl Biol.* **89**, 179–195.

Le Douarin, N. M. (1984). Cell migration in embryos. *Cell.* **38**, 353–360.

Löfberg, J. and Ahlfors, K. (1978). Extracellular matrix organization and early neural crest cell migration in the axolotl embryo. In *Formshaping Movements in Neurobiology* (eds C.-O. Jacobsson, and T. Ebendal), pp. 87–101. Almqvist and Wiksell, Stockholm.

Löfberg, J., Ahlfors, K. and Fällström, C. (1980). Neural crest

cell migration in relation to extracellular matrix organization in the embryonic axolotl trunk. *Devl Biol.* **75**, 148–167.

LÖFBERG, J., EPPERLEIN, H. H., PERRIS, R. AND STIGSON, M. (1989*a*). Neural crest cell migration in the axolotl embryo: A pictorial essay. In *The Developmental Biology of the Axolotl* (eds. J. B. Armstrong and G. M. Malacinski). Oxford, Oxford University Press.

LÖFBERG, J., NYNÄS-MCCOY, A., OLSSON, C., JÖNSSON, L. AND PERRIS, R. (1985). Stimulation of initial neural crest cell migration in the axolotl embryo by tissue grafts and extracellular matrix transplanted on microcarriers. *Devl Biol.* **107**, 442–459.

LÖFBERG, J., PERRIS, R. AND EPPERLEIN, H. H. (1989*b*). Regulation of neural crest cell migration: Retarded "maturation" of regional extracellular matrix inhibits pigment cell migration in embryos of the white axolotl mutant. *Devl Biol.* **131**, 168–181.

MARTINS-GREEN, M. AND ERICKSON, C. A. (1987). Basal lamina is not a barrier to neural crest cell emigration: documentation by TEM and by immunofluorescent and immunogold labelling. *Development* **101**, 517–533.

MCLEAN, I. W. AND NAKANE, P. K. (1974). Periodate-lysine-paraformaldehyde fixative, a new fixative for immunoelectron microscopy. *J. Histochem. Cytochem.* **22**, 1077–1083.

NEUKIRCHEN, R. O., SCHLOSSHAUER, B., BAARS, S., JÄCKLE, H. AND SCHWARZ, U. (1982). Two-dimensional protein analysis on a microscale. *J. biol. Chem.* **257**, 15229–15234.

NEWGREEN, D. F. (1982). Adhesion to extracellular materials by neural crest cells at stage of initial migration. *Cell Tissue Res.* **227**, 297–317.

NEWGREEN, D. F. (1989). Physical influences on neural crest cell migration in avian embryos: contact guidance and spatial restriction. *Devl Biol.* **131**, 136–148.

NEWGREEN, D. F. AND ERICKSON, C. A. (1986). The migration of neural crest cells. *Int. Rev. Cytol.* **10**, 89–145.

NEWGREEN, D. F., SCHEEL, M. AND KASTNER, V. (1986). Morphogenesis of sclerotome and neural crest in avian embryos. *In vivo* and *in vitro* studies on the role of notochordal extracellular matrix. *Cell Tissue Res.* **244**, 299–313.

PAYETTE, R. F., TENNYSON, V. M., POMERANZ, H. D., PHAM, T. D., ROTHMAN, T. P. AND GERSHON, M. D. (1988). Accumulation of components of basal laminae: Association with the failure of neural crest cells to colonize the presumptive aganglionic bowel of Is/Is mutant mice. *Devl Biol.* **125**, 341–360.

PERRIS, R. AND BRONNER-FRASER, M. (1989*a*). Recent advances in defining the role of the extracellular matrix in neural crest development. *Comm. Dev. Neurobiol.* **1**, 61–83.

PERRIS, R. AND JOHANSSON, S. (1987). Amphibian neural crest cell migration on purified extracellular matrix components: A chondroitin sulfate proteoglycan inhibits locomotion on fibronectin substrates. *J. Cell Biol.* **105**, 2511–2521.

PERRIS, R. AND JOHANSSON, S. (1990). Inhibition of neural crest cell migration by aggregating chondroitin sulfate proteoglycans is mediated by their hyaluronan-binding domains. *Devl Biol.* **137**, 1–12.

PERRIS, R., KROTOSKI, D., DOMINGO, C., LALLIER, T., SORRELL, J. M. AND BRONNER-FRASER, M. (1990). Distribution of hyaluronan and proteoglycans during avian neural crest development. Submitted.

PERRIS, R. AND LÖFBERG, J. (1986). Promotion of chromatophore differentiation in isolated premigratory neural crest cells by extracellular material explanted on microcarriers. *Devl Biol.* **113**, 327–341.

PERRIS, R., PAULSSON, M. AND BRONNER-FRASER, M. (1989*b*). Molecular mechanisms of neural crest cell migration on fibronectin and laminin. *Devl Biol.* **136**, 222–238.

SAINT-MARIE, G. A. (1962). A paraffin embedding technique for studies employing immunofluorescence. *J. Histohem. Cytochem.* **10**, 250–256.

SANDERS, E. J. (1979). Development of the basal lamina and extracellular materials in the early chick embryo. *Cell Tissue Res.* **198**, 527–537.

SCOTT, J. E. (1985). Proteoglycan histochemisty – A valuable tool for connective tissue biochemists. *Collagen Rel. Res.* **5**, 41–75.

SPIETH, J. AND KELLER, R. E. (1984). Neural crest cell behavior in white and dark larvae of Ambystoma mexicanum: Differences in cell morphology, arrangement, and extracellular matrix as related to migration. *J. exp. Zool.* **229**, 91–107.

TAN, S. S., CROSSIN, K. L., HOFFMAN, S. AND EDELMAN, G. M. (1987). Asymmetric expression in somites of cytotactin and its proteoglycan ligand is correlated with neural crest cell distribution. *Proc. natn. Acad. Sci. U.S.A.* **84**, 7977–7981.

TUCKER, R. P. (1986). The role of glycosaminoglycans in anuran pigment cell migration. *J. Embryol. exp. Morph.* **92**, 145–164.

TUCKER, R. P. AND ERICKSON, C. A. (1986). Pigment cell pattern formation in Taricha torosa: The role of the extracellular matrix in controlling pigment cell migration and differentiation. *Devl Biol.* **104**, 390–405.

TUCKETT, F. AND MORRISS-KAY, G. (1988). Alcian Blue staining of glycosaminoglycans in embryonic material: effect of different fixatives. *Histochem. J.* **20**, 174–182.

TURLEY, E. A., ERICKSON, C. A. AND TUCKER, R. P. (1985). The retension and ultrastructural appearances of various extracellular matrix molecules incorporated into three-dimensional hydrated collagen lattices. *Devl Biol.* **109**, 347–369.

VON BOXBERG, Y. (1988). Protein analysis on two-dimensional polyacrylamide gels in the femtogram range: Use of the new sulfur-labelling reagent 35SLR. *Anal. Biochem.* **169**, 372–375.

WIESLANDER, J., LANGEVELD, J., BUTKOVSKI, R., JODLOVSKI, M., NOELKEN, M. AND HUDSON, B. G. (1985). Physical and immunochemical studies of the globular domain of type IV collagen. *J. biol. Chem.* **260**, 8564–8570.

(*Accepted 5 March 1990*)